

# Effective Interaction between the inter-penetrating Kagomé lattices in $\text{Na}_x\text{CoO}_2$

Martin Indergand,<sup>1</sup> Yasufumi Yamashita,<sup>2</sup> Hiroaki Kusunose,<sup>3</sup> and Manfred Sigrist<sup>1</sup>

<sup>1</sup>*Theoretische Physik, ETH-Hönggerberg, CH-8093 Zürich, Switzerland*

<sup>2</sup>*Institute for Molecular Science, National Institutes of Natural Sciences, Okazaki 444-8585, Japan*

<sup>3</sup>*Physics Department, Tohoku University, Sendai 980-8578 Japan*

(Dated: March 23, 2022)

A multi-orbital model for a  $\text{CoO}_2$ -layer in  $\text{Na}_x\text{CoO}_2$  is derived. In this model the kinetic energy for the degenerate  $t_{2g}$ -orbitals is given by indirect hopping over oxygen, leading naturally to the concept of four inter-penetrating Kagomé lattices. Local Coulomb interaction couples the four lattices and an effective Hamiltonian for the interaction in the top band can be written in terms of fermionic operators with four different flavors. Focusing on charge and spin density instabilities, a big variety of possible metallic states with spontaneously broken symmetry are found. These states lead to different charge, orbital, spin and angular momentum ordering patterns. The strong superstructure formation at  $x = 0.5$  is also discussed within this model.

## I. INTRODUCTION

The layered  $\text{Na}_x\text{CoO}_2$  has been initially studied for its extraordinary thermoelectric properties and for its interesting dimensional crossover.<sup>1,2,3,4</sup> But recently wider attention has been triggered by the discovery of superconductivity in hydrated  $\text{Na}_{0.35}\text{CoO}_2$  and the discovery of an insulating phase in  $\text{Na}_{0.5}\text{CoO}_2$ .<sup>5,6,7,8</sup> Since then, various types of charge ordering phenomena in  $\text{Na}_x\text{CoO}_2$  have been reported,<sup>9,10,11,12,13,14,15,16,17,18,19,20,21,22</sup> but also strong spin-fluctuations and spin density wave transitions have been observed.<sup>23,24,25,26,27,28,29,30,31,32,33,34</sup>

The material consists of  $\text{CoO}_2$ -layers where Co-ions are enclosed in edge-sharing O-octahedra. These layers alternate with the Na-ion layers with Na entering as  $\text{Na}^{1+}$  and donating one electron each to the  $\text{CoO}_2$ -layer.

The electronic properties are dominated by the  $3d$ - $t_{2g}$  electrons of the Co-ions which form a two-dimensional triangular lattice. However, the spatial arrangement of the  $\text{Na}^{1+}$ -ions plays a crucial role too for the physics of this material. There are two basic positions for the Na-ions, one directly above or below a Co-site and another in a center position of a triangle spanned by the Co-lattice. The metallic properties are unusual and vary with the Na-concentration and arrangement.

A brief overview of the present knowledge of the phase diagram of  $\text{Na}_x\text{CoO}_2$  leads to following still rough picture. The most salient and robust feature, at first sight is the charge ordered phase for  $x = 0.5$  separating the Na-poor from the Na-rich system. The Na-ions arrange in a certain pattern inducing an insulating magnetic phase in the  $\text{CoO}_2$ -layers below 50K.<sup>33</sup> On the Na-poor side ( $x < 0.5$ ) the compound behaves like a paramagnetic metal. When it is intercalated with  $\text{H}_2\text{O}$  superconductivity appears between  $x \approx 0.25$  and  $x \approx 0.35$ . In several respects more interesting is the Na-rich side where one finds a so-called Curie-Weiss metal. Here the magnetic susceptibility displays a pronounced Curie-Weiss-like behavior after subtracting an underlying temperature independent part:  $\chi = C/(T - \Theta)$  where  $\Theta$  ranges roughly between -50 and -200 K depending on  $x$ , and the Curie constant

is consistent with a magnetic moment in the range of 1 - 1.7  $\mu_B$ . Note that deviations from the Curie-Weiss behavior have been observed at low temperatures.<sup>35</sup> On the Na-rich side a transition at high temperature  $\sim 250 - 340$  K has been observed and interpreted as crystal structure or charge ordering<sup>15,18,27</sup>. For  $\text{Na}_{0.75}\text{CoO}_2$  a magnetic transition occurs at 22 K and is most likely a commensurate spin density wave or ferrimagnetic order which is rather soft towards magnetic polarization.<sup>26,27,28,29</sup> Interestingly this magnetic phase is metallic and has even a higher mobility than the non-magnetic phase. For Na-content  $x \geq 0.75$  several magnetic transition at a similar critical temperatures have been observed, but  $\mu\text{SR}$ -data suggest rather an incommensurate spin density wave order<sup>28,29,34</sup>.

The arrangement of the Na ions between the layers depends on the Na doping  $x$  and several superstructures have been found,<sup>9,10</sup> the clearest evidence for the superstructure formation is at  $x = 0.5$  where the Na-ordering leads to a metal-insulator transition at low temperatures.<sup>7,8,12</sup> But also away from  $x = 0.5$ , NMR experiments indicate the existence of non equivalent cobalt sites and phase separation.<sup>14,16</sup>

The complex interplay between Na-arrangement and the electronic properties poses a interesting problem. Various theoretical studies have mainly focused on single band models on the frustrated triangular lattice, in particular in connection with the superconducting phase ignoring Na-potentials.<sup>36,37,38,39,40,41,42</sup> There is also work done on multi-orbital models<sup>43,44</sup> and density functional calculations have been performed.<sup>45,46,47,48,49,50,51,52</sup> According to LDA calculations, the Fermi surface lies near the top of the  $3d$ - $t_{2g}$ -bands. They form a large hole-like Fermi surface of predominantly  $a_{1g}$  character in agreement with ARPES experiments.<sup>53,54,55</sup> In addition the LDA calculations suggest, that smaller hole pockets with mixed  $a_{1g}$  and  $e'_g$  character exist on the  $\Gamma - K$  direction on the Na-poor side.

At the  $\Gamma$  point the states with  $a_{1g}$  and  $e'_g$  symmetry are clearly split, but on average over the entire Brillouin zone the mixing between  $a_{1g}$  and  $e'_g$  is substantial. Koshibae and Maekawa argued that the splitting at the  $\Gamma$  point

originates from the cobalt-oxygen hybridization rather than from a crystal field effect due to the distortion of the oxygen octahedra, because the crystal field effect in a simple ionic picture would lead to the opposite splitting of the  $a_{1g}$  and  $e'_g$  states.<sup>43</sup> There is also spectral evidence, that the low-energy excitations of  $\text{Na}_x\text{CoO}_2$  have significant O  $2p$  character.<sup>56</sup> Reproducing the LDA Fermi surface with a tight binding fit for the Co  $t_{2g}$  orbitals, it turns out that the direct overlap integral between the cobalt orbitals is much smaller than the indirect hopping integral over the oxygen  $2p$  orbitals.<sup>44</sup> Therefore, it is reasonable to start with a three band tight binding model of degenerate  $t_{2g}$  orbitals, where the only hopping processes are indirect hopping processes over intermediate oxygen orbitals. This approximation provides an interesting system of four independent and inter-penetrating Kagomé lattices as it was already pointed out by Koshibae and Maekawa.

Our study will be based on this model band structure which has a high symmetry. Within this model we examine various forms of order that could be possible from onsite Coulomb interaction. The paper is organized as follows: In section II, the tight-binding model and the concepts of Kagomé operators and pocket operators are introduced. In section III an effective Hamiltonian for the local Coulomb interaction is derived and in section IV this effective interaction is written in a diagonal form, by choosing an appropriate basis of  $\text{SU}(4)$  generators. In section V, the effects of small deviations from our simplified tight-binding model are discussed. In section VI, all possible charge and spin ordering patterns of our model and the corresponding phase transitions, are shortly described. In section VII the relevance of the above described collective degrees of freedom to  $\text{Na}_x\text{CoO}_2$  is discussed by comparing the different coupling constants and by taking into account symmetry lowering effects. In section VIII we apply our model to the Na-ordering observed at  $x = 0.5$  and we summarize and conclude in section IX.

## II. TIGHT-BINDING MODEL

We base our model on the assumption that the  $3d$ - $t_{2g}$ -orbitals on the Co-ions are degenerate. Their electrons disperse only via  $\pi$ -hybridization with the intermediate oxygens occupying the surrounding octahedra (Fig.1). As noticed by Koshibae and Maekawa the resulting electronic structure corresponds to a system of four decoupled equivalent electron systems of electrons hopping on a Kagomé lattice<sup>43</sup>. The different sites, however, are represented by different orbitals. Each of the three orbitals  $\{d_{yz}, d_{zx}, d_{xy}\}$  on a given site participate in one Kagomé lattice, and the fourth Kagomé lattice has a void on this site. The corresponding tight-binding model has the following form,

$$H_{\text{tb}} = \sum_{\mathbf{k}\sigma} \sum_{mm'} \epsilon_{\mathbf{k}}^{mm'} c_{\mathbf{k}m\sigma}^\dagger c_{\mathbf{k}m'\sigma} \quad (1)$$

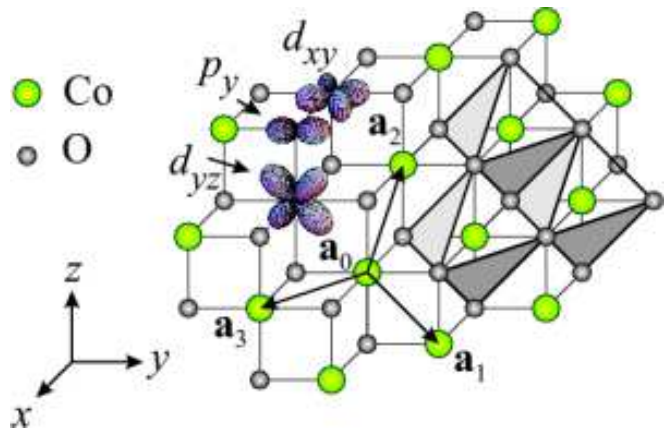


FIG. 1: Schematic figure of a  $\text{CoO}_2$  plane drawn with cubic unit cells. The edge-sharing of the oxygen octahedra around the Co ions is visualized. The edges of the cubes are oriented along the coordinate system  $(x, y, z)$ . The triangular lattice of the cobalt is spanned by the vectors  $\mathbf{a}_1, \mathbf{a}_2, \mathbf{a}_3$ . ( $\mathbf{a}_1 + \mathbf{a}_2 = -\mathbf{a}_3$ ).  $a = |\mathbf{a}_i|$  is the lattice spacing. An oxygen  $2p$  orbital and the cobalt  $t_{2g}$  orbitals hybridizing with it by  $\pi$ -hybridization, are shown.

where  $c_{\mathbf{k}m\sigma}^\dagger = \frac{1}{\sqrt{N}} \sum_{\mathbf{r}} e^{i\mathbf{k}\cdot\mathbf{r}} c_{\mathbf{r}m\sigma}^\dagger$  are the operators in momentum space of  $c_{\mathbf{r}m\sigma}^\dagger$  which creates a  $t_{2g}$ -orbital ( $d_{yz}, d_{zx}, d_{xy}$ ) with index  $m \in \{1, 2, 3\}$  and spin  $\sigma \in \{\uparrow, \downarrow\}$  on the cobalt-site  $\mathbf{r}$ .  $N$  is the number of Co-sites in the lattice.

$$\hat{\epsilon}_{\mathbf{k}} = \begin{pmatrix} -\mu & 2t \cos(k_3) & 2t \cos(k_2) \\ 2t \cos(k_3) & -\mu & 2t \cos(k_1) \\ 2t \cos(k_2) & 2t \cos(k_1) & -\mu \end{pmatrix}, \quad (2)$$

with  $k_i = \mathbf{k} \cdot \mathbf{a}_i$ , cf. Fig. 1. The hopping parameter  $t = t_{pd}^2/\Delta > 0$ , where  $t_{pd}$  is the hopping integral between the  $p_y$  and the  $d_{xy}$  or  $d_{yz}$  orbital shown in Fig. 1.  $\Delta$  is the energy difference between the oxygen  $p$  and the Co- $t_{2g}$  levels. The diagonalization of the matrix  $\hat{\epsilon}_{\mathbf{k}}$  by a rotation matrix  $\hat{O}_{\mathbf{k}} \in \text{SO}(3)$

$$\sum_{mm'} O_{\mathbf{k}}^{im} \epsilon_{\mathbf{k}}^{mm'} O_{\mathbf{k}}^{jm'} = \delta_{ij} E_{\mathbf{k}}^i \quad (3)$$

results in the three energy bands

$$\begin{aligned} E_{\mathbf{k}}^1 &= t + t\sqrt{1 + 8 \cos(k_1) \cos(k_2) \cos(k_3)} - \mu \\ E_{\mathbf{k}}^2 &= t - t\sqrt{1 + 8 \cos(k_1) \cos(k_2) \cos(k_3)} - \mu \\ E_{\mathbf{k}}^3 &= -2t - \mu. \end{aligned} \quad (4)$$

These bands have the periodicity  $E_{\mathbf{k}+\mathbf{B}_j}^l = E_{\mathbf{k}}^l$ , where the vectors  $\mathbf{B}_j$  are defined by

$$\mathbf{a}_i \cdot \mathbf{B}_j = \frac{2\pi}{\sqrt{3}} \sin(\theta_i - \theta_j) \quad i, j \in \{1 \dots 3\} \quad (5)$$

with  $\theta_j = 2\pi j/3$ . These three vectors  $\mathbf{B}_j$  connect the  $\Gamma$  point with the three M points in the Brillouin zone (BZ),

and the vectors  $2\mathbf{B}_j$  are primitive reciprocal lattice vectors. The bands of this tight-binding model have therefore a higher periodicity than the bands of a more general model. This leads to the appearance of special symmetry lines (thin lines) and symmetry points (M' and K') in the Brillouin zone, shown in Fig. 2, where the bands are plotted along the line  $\Gamma'$ -K'-M'- $\Gamma'$ . Within a reduced BZ, these bands correspond to the bands of a nearest neighbor tight-binding model on a Kagomé lattice<sup>43</sup>. The density of states per spin and per reduced BZ is also shown in Fig. 2. It has a logarithmic singularity at  $E = 2t$  and jumps from  $\sqrt{3}/(2\pi t)$  to 0 at  $E = 4t$ .

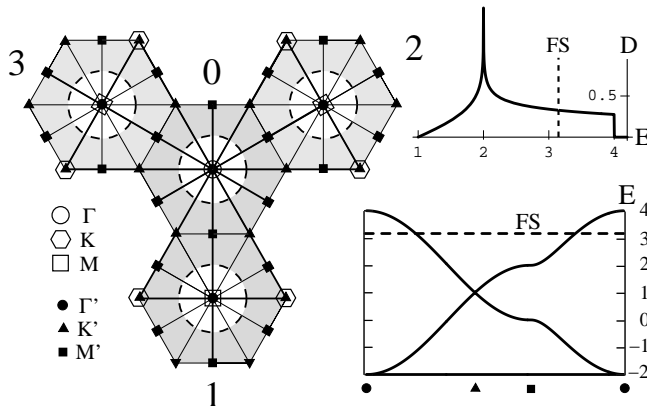


FIG. 2: The original Brillouin zone (BZ) of the triangular lattice consists of four reduced BZs around of the  $\Gamma$  point (0) and the three M points (1,2,3). The symmetry points of the reduced BZs, M', K' and  $\Gamma'$  are symmetry points for the tight binding model in Eq. (1) due to the higher periodicity of the bands. It is therefore sufficient to draw the bands along the lines  $\Gamma'$ -K'-M'- $\Gamma'$ . The Fermi surface (FS) for  $x = 0.5$  lies at  $E_{\mathbf{k}}^1 \approx 3.16t$ . The density of states per spin and per reduced Brillouin zone  $D$  is given in units of  $1/t$ . It has a logarithmic singularity at  $E = 2t$ .

The states, that are connected by the considered hopping processes form a Kagomé lattice. Since in this way the  $\text{CoO}_2$ -plane consists of four independent and interpenetrating Kagomé lattices<sup>43</sup>, it is convenient to label the states belonging to the same Kagomé lattice with an index  $l \in \{0, 1, 2, 3\}$ . This can be done with the vectors  $\mathbf{a}_l$  of Fig. 1 as

$$a_{\mathbf{R}m}^{\dagger l} = c_{\mathbf{R}+\mathbf{a}_l+\mathbf{a}_m}^{\dagger}. \quad (6)$$

In this way, the operators  $a_{\mathbf{R}m}^{\dagger l}$  with fixed  $l$  create all the states off a Kagomé lattice. In the following, these operators will be called *Kagomé operators*. Their Fourier transform is given by

$$a_{\mathbf{k}m}^{\dagger l} = \frac{2}{\sqrt{N}} \sum_{\mathbf{R}} e^{i\mathbf{k} \cdot (\mathbf{R} + \mathbf{a}_l + \mathbf{a}_m)} a_{\mathbf{R}m}^{\dagger l}, \quad (7)$$

where the vectors  $\mathbf{k}$  belong to the reduced BZ, labeled 0 in Fig. 2 and  $\mathbf{R}$  runs over the lattice spanned by the vectors  $2\mathbf{a}_i$ .

The BZ consists of four reduced BZs shown in Fig. 2. An alternative labeling of the states is obtained therefore by defining the operators

$$b_{\mathbf{k}m}^{\dagger j} = e^{-i\mathbf{B}_j \cdot \mathbf{a}_m} c_{\mathbf{k}+\mathbf{B}_j m}^{\dagger}, \quad (8)$$

where the vectors  $\mathbf{B}_j$  are defined in Eq. (5) and in addition we set  $\mathbf{B}_0 = 0$ . As shown in Eq. (A1) of Appendix A, the transformation between the Kagomé operators  $a_{\mathbf{k}}^{\dagger l}$  and the *pocket operators*  $b_{\mathbf{k}}^{\dagger j}$  corresponds to a discrete Fourier transformation of a  $2 \times 2$  lattice, and is given by

$$b_{\mathbf{k}m}^{\dagger j} = \frac{1}{2} \sum_l e^{i\mathbf{B}_j \cdot \mathbf{a}_l} a_{\mathbf{k}m}^{\dagger l} = \sum_l \mathcal{F}_{jl} a_{\mathbf{k}m}^{\dagger l}, \quad (9)$$

where we have defined the symmetric and orthogonal  $4 \times 4$  matrix

$$\mathcal{F}_{jl} = \mathcal{F}_{lj} = \mathcal{F}_{j'l}^* = \mathcal{F}_{jl}^{-1} = \frac{1}{2} e^{i\mathbf{B}_j \cdot \mathbf{a}_l}. \quad (10)$$

Note that the matrix elements of  $\mathcal{F}$  are  $\pm 1/2$ , as the scalar products  $\mathbf{B}_j \cdot \mathbf{a}_l$  of Eq. (5) equal 0 or  $\pm\pi$ .

The tight-binding Hamiltonian (1) is diagonal in the pocket indices  $j$  (cf. Appendix A Eq. (A2)),

$$H_{\text{tb}} = \sum_{l\mathbf{k}\sigma} \sum_{mm'} \epsilon_{\mathbf{k}}^{mm'} b_{\mathbf{k}m\sigma}^{\dagger l} b_{\mathbf{k}m'\sigma}^l. \quad (11)$$

From this expression it is apparent, that the tight-binding Hamiltonian is invariant under any  $U(4)$  transformation of the of the form

$$b_{\mathbf{k}m\sigma}^{\dagger j} \rightarrow \tilde{b}_{\mathbf{k}m\sigma}^{\dagger j} = \sum_{j'} U_{jj'} b_{\mathbf{k}m\sigma}^{\dagger j'}. \quad (12)$$

Eq. (9) is just a special case of Eq. (12). This shows that  $H_{\text{tb}}$  is also diagonal in the Kagomé indices.

It is important to notice that the transformations in Eq. (12) involves symmetries that are not present in a more general tight-binding model. For example a finite hopping integral  $t_{dd}$  due to the  $\sigma$ -hybridization between neighboring  $t_{2g}$ -orbitals would break this symmetry. We will discuss this aspect below in more detail and remain for the time being in this high-symmetry situation.

In  $\text{Na}_x\text{CoO}_2$  the lower two bands are completely filled and will be quite inert. For this reason in the following sections we will only deal with the operators of the top band  $E_{\mathbf{k}}^1$  whose operators are denoted as

$$a_{\mathbf{k}\sigma}^{\dagger l} = \sum_m O_{\mathbf{k}}^{1m} a_{\mathbf{k}m\sigma}^{\dagger l} \quad \text{and} \quad b_{\mathbf{k}\sigma}^{\dagger j} = \sum_m O_{\mathbf{k}}^{1m} b_{\mathbf{k}m\sigma}^j, \quad (13)$$

resp., where  $O_{\mathbf{k}}^{1m}$  are matrix elements of the rotation matrix  $\hat{O}_{\mathbf{k}}$  of Eq. (3).

The top band gives rise to four identical Fermi surface pockets in the BZ, one in the  $\Gamma$ -point and three at the M-points. A translation in the reciprocal space by the vectors  $\mathbf{B}_j$  maps the pocket around the  $\Gamma$  point onto a pocket around the M-point. However, this fact does not

lead to nesting singularities in the susceptibility because a hole pocket is mapped onto a hole pocket by the vector  $\mathbf{B}_j$ . The susceptibility of the top band is given by

$$\chi_q^o = \frac{1}{N} \sum_k \frac{f_{k+q} - f_k}{E_k^1 - E_{k+q}^1} = \frac{4}{N} \sum_{\mathbf{\kappa}} \frac{f_{\mathbf{\kappa}+\mathbf{Q}} - f_{\mathbf{\kappa}}}{E_{\mathbf{\kappa}}^1 - E_{\mathbf{\kappa}+\mathbf{Q}}^1}, \quad (14)$$

where  $f_k = f(\beta(E_k^1 - \mu))$  and  $f$  is the Fermi-function. In the last expression of Eq. (14), the sum over  $\mathbf{\kappa}$  is restricted to the reduced BZ.  $\mathbf{Q}$  also lies in the reduced BZ and is given by  $\mathbf{Q} = q + \mathbf{B}_j$ . The susceptibility  $\chi_q^o = \chi_{\mathbf{Q}}^o$  is periodic with respect to the reduced BZ and is just four times the susceptibility of a single Kagomé lattice. As we have almost circular hole pockets with quadratic dispersion around the  $\Gamma$  and the M points, the susceptibility is therefore approximately given by the susceptibility of the free electron gas in two dimensions within each reduced BZ, with circular plateaus of radius  $2\kappa_F$  around the  $\Gamma$  and the three M points.

### III. COULOMB INTERACTION

In this section we introduce the Coulomb interaction between the electrons. As we have spin and orbital degrees of freedom, the on-site Coulomb interaction consists of intra-orbital repulsion  $U$ , inter-orbital repulsion  $U'$ , Hund's coupling  $J_H$  and a pair hopping term  $J'$ . These parameters are related by  $U \approx U' + 2J_H$  and  $J_H = J'$ , where the first relation is exact for spherical symmetry. We can write the onsite Coulomb interaction as

$$\begin{aligned} H_{\mathbf{r}}^C &= U \sum_m n_{\mathbf{r}m\uparrow} n_{\mathbf{r}m\downarrow} + \frac{U'}{2} \sum_{m \neq m'} \sum_{\sigma\sigma'} n_{\mathbf{r}m\sigma} n_{\mathbf{r}m'\sigma'} \\ &+ \frac{J_H}{2} \sum_{m \neq m'} \sum_{\sigma\sigma'} c_{\mathbf{r}m\sigma}^\dagger c_{\mathbf{r}m'\sigma'}^\dagger c_{\mathbf{r}m\sigma'} c_{\mathbf{r}m'\sigma} \\ &+ \frac{J'}{2} \sum_{m \neq m'} \sum_{\sigma \neq \sigma'} c_{\mathbf{r}m\sigma}^\dagger c_{\mathbf{r}m'\sigma'}^\dagger c_{\mathbf{r}m'\sigma} c_{\mathbf{r}m\sigma}, \end{aligned} \quad (15)$$

where  $n_{\mathbf{r}m\sigma} = c_{\mathbf{r}m\sigma}^\dagger c_{\mathbf{r}m\sigma}$ . We obtain an effective Hamiltonian for the Coulomb interaction by rewriting the Hamiltonian in terms of the pocket operators of the top band  $b_{\mathbf{\kappa}\sigma}^{\dagger l}$  defined in Eq. (13). For small  $\kappa = |\mathbf{\kappa}|a$  we can expand Eq. (13) in powers of  $\kappa^2$  and obtain up to terms of the order  $\kappa^2$

$$b_{\mathbf{\kappa}\sigma}^{\dagger j} = \frac{1}{\sqrt{3}} \sum_m \left( 1 + \frac{\kappa^2}{12} \cos[2(\theta - \theta_m)] \right) b_{\mathbf{\kappa}m\sigma}^j, \quad (16)$$

where  $\theta_m = 2\pi m/3$ . Expanding the energy of the top band around the point  $\Gamma'$ , we obtain

$$\epsilon_{\mathbf{\kappa}}^1 = t(4 - \kappa^2 + \frac{\kappa^4}{12} - \frac{\kappa^6}{360} \cos(6\theta) + O(\kappa^8)). \quad (17)$$

This shows that the pockets around the points  $\Gamma'$  are almost perfectly circular. The radius  $\kappa_F/a$  of these pockets

$9C = -3U + 2J' + 2J_H + 2U'$	$9D = +3U + 6J' - 2J_H - 2U'$
$9E^c = +3U - 2J' - 10J_H + 14U'$	$9E^s = -3U + 2J' - 6J_H + 2U'$
$9F^c = +3U - 2J' + 14J_H - 10U'$	$9F^s = -3U + 2J' + 2J_H - 6U'$

TABLE I: The coefficients of Eq. (20)

depends on the Na doping  $x$ . Note that  $x$  corresponds to the density of carriers with  $x = 1$  giving a completely filled top band. We have  $\kappa_F^2 = \pi(1-x)/\sqrt{3}$ . For the interaction in weak-coupling and at low temperatures, the states near the Fermi surface are important. For these states and for not too small Na doping  $x$  we can neglect the second term in the parenthesis of Eq. (16) compared to 1. Note, that this condition on  $x$  is not very restrictive. Even for  $x = 0.35$  the second term together with all higher order terms is on the average one order of magnitude smaller than 1. Dropping the second term in Eq. (16) spreads the  $a_{1g}$  symmetry of the states  $b_{\mathbf{\kappa}\sigma}^{\dagger j}$ , which is exact only for  $\mathbf{\kappa} = 0$ , to all relevant states in the top band. The interaction (15) can now be rewritten in terms of the  $a_{1g}$  symmetric operators  $b_{\mathbf{\kappa}\sigma}^{\dagger j}$ . Processes involving states of the filled lower bands are dropped. The dropping of the second term in the parenthesis of Eq. (16) is a considerable simplification because it removes all  $\mathbf{\kappa}$ -dependence of the potential.

At this point it is convenient to introduce density and spin density operators for the pocket operators of the top band.

$$\begin{aligned} \hat{n}_{\mathbf{Q}}^{ij} &= \frac{4}{N} \sum_{\mathbf{\kappa}\sigma} b_{\mathbf{\kappa}+\mathbf{Q}\sigma}^{\dagger i} b_{\mathbf{\kappa}\sigma}^j \\ \hat{\mathbf{S}}_{\mathbf{Q}}^{ij} &= \frac{2}{N} \sum_{\mathbf{\kappa}\sigma\sigma'} b_{\mathbf{\kappa}+\mathbf{Q}\sigma}^{\dagger i} \boldsymbol{\sigma}_{\sigma\sigma'} b_{\mathbf{\kappa}\sigma}^j \end{aligned} \quad (18)$$

The resulting effective interaction can be expressed with these operators in the following way

$$H_{\text{eff}} = \frac{N}{32} \sum_{\mathbf{Q}} \left( B_{ijkl}^s \hat{\mathbf{S}}_{\mathbf{Q}}^{ij} \hat{\mathbf{S}}_{-\mathbf{Q}}^{lk} + \frac{1}{4} B_{ijkl}^c \hat{n}_{\mathbf{Q}}^{ij} \hat{n}_{-\mathbf{Q}}^{lk} \right). \quad (19)$$

The symbols  $B^{c/s}$  depend on the Coulomb integrals and are given by

$$\begin{aligned} B_{ijkl}^{c/s} &= \pm C(2\delta_{ijkl} - \epsilon_{ijkl}^2) \pm D\delta_{il}\delta_{jk} \\ &+ E^{c/s}\delta_{ij}\delta_{kl} + F^{c/s}\delta_{ik}\delta_{jl}, \end{aligned} \quad (20)$$

where the  $\delta$  ( $\epsilon^2$ ) symbol equals 1, if all the indices are equal (different) and 0 otherwise. The coefficients  $C$ ,  $D$ ,  $E^{c/s}$  and  $F^{c/s}$  are listed in TABLE I. Note, that for small pockets, the momenta  $\mathbf{\kappa}$  of the pocket operators  $b_{\mathbf{\kappa}}^j$  in the four fermion terms of Eq (19) can not add up to a half a reciprocal lattice vector  $\mathbf{B}_i$ . In order to conserve momentum they must therefore add up to zero. Due to the position of the pockets in the BZ, Umklapp processes with low energy transfer are however possible

for arbitrary small pockets. In fact, the processes proportional to  $\epsilon_{ijkl}^2$  and  $\delta_{il}\delta_{jk}(1 - \delta_{ij})$  are Umklapp processes, as  $\mathbf{B}_i - \mathbf{B}_j + \mathbf{B}_l - \mathbf{B}_k$  is a non-vanishing reciprocal lattice vector for  $\epsilon_{ijkl} \neq 0$  and for  $\delta_{il}\delta_{jk}(1 - \delta_{ij}) \neq 0$ , and from Eq. (8) the momentum created by the operator  $b_{\mathbf{K}}^{\dagger j}$  is  $\mathbf{K} + \mathbf{B}_j$ .

Some details about the derivation of Eq. (19) are provided in Appendix B. There are different ways of writing this interaction in terms of the operators in (18). Our formulation treats charge- and spin degrees of freedom in the same way. It corresponds to the decomposition of a Hubbard interaction  $n_{\uparrow}n_{\downarrow}$  into  $\frac{1}{2}(\frac{1}{4}n^2 - \mathbf{S} \cdot \mathbf{S})$ .

In order to express the effective interaction Hamiltonian of Eq. (19) in terms of the Kagomé operators  $a_{\mathbf{K}\sigma}^l$ , we define spin and charge density operators from the Kagomé operators  $a_{\mathbf{K}\sigma}^l$  as in Eq. (18).

$$\begin{aligned} n_{\mathbf{Q}}^{ij} &= \frac{4}{N} \sum_{\mathbf{K}\sigma} a_{\mathbf{K}+\mathbf{Q}\sigma}^{\dagger i} a_{\mathbf{K}\sigma}^j \\ \mathbf{S}_{\mathbf{Q}}^{ij} &= \frac{2}{N} \sum_{\mathbf{K}\sigma\sigma'} a_{\mathbf{K}+\mathbf{Q}\sigma}^{\dagger i} \boldsymbol{\sigma}_{\sigma\sigma'} a_{\mathbf{K}\sigma}^j \end{aligned} \quad (21)$$

Note, that the density operators, which are defined from the pocket operators  $b_{\mathbf{K}\sigma}^l$  are marked by a hut. The effective Hamiltonian,  $H_{\text{eff}}$ , of Eq. (19) can be rewritten as

$$H_{\text{eff}} = \frac{N}{32} \sum_{\mathbf{Q}} \left( A_{ijkl}^s \mathbf{S}_{\mathbf{Q}}^{ij} \mathbf{S}_{-\mathbf{Q}}^{lk} + \frac{1}{4} A_{ijkl}^c n_{\mathbf{Q}}^{ij} n_{-\mathbf{Q}}^{lk} \right). \quad (22)$$

From Eq. (9) and (10) follows that

$$A_{ijkl}^{c/s} = \mathcal{F}_{im} \mathcal{F}_{jn} \mathcal{F}_{ko} \mathcal{F}_{lp} B_{mnop}^{c/s}. \quad (23)$$

The symbols  $A^{c/s}$  turn out to have a simpler structure, given by

$$\begin{aligned} A_{ijkl}^c &= \frac{8}{9} \left[ -\frac{C}{2} \delta_{ijkl} + J' \delta_{il} \delta_{jk} + (2U' - J_{\text{H}}) \delta_{ij} \delta_{kl} + \right. \\ &\quad \left. + (2J_{\text{H}} - U') \delta_{ik} \delta_{jl} \right], \\ A_{ijkl}^s &= \frac{8}{9} \left[ +\frac{C}{2} \delta_{ijkl} - J' \delta_{il} \delta_{jk} - J_{\text{H}} \delta_{ij} \delta_{kl} - U' \delta_{ik} \delta_{jl} \right]. \end{aligned} \quad (24)$$

#### IV. SU(4) GENERATORS

The tight-binding Hamiltonian described in section II has a  $U(4)$  symmetry, reflecting the fact that it consists of 4 independent and equivalent Kagomé lattices. The correlations introduced by the on-site Coulomb repulsion in Eq. (15) breaks this symmetry and leads to interaction between orbitals belonging to different Kagomé lattices, as the three  $t_{2g}$ -orbitals on a given Co-site belong to three different Kagomé lattices. The effective Hamiltonian in Eq. (19) is not invariant under general  $U(4)$  transformations, but is still invariant under a finite subgroup of

$U(4)$ . The symbols  $A_{ijkl}^{c/s}$  defined in Eq. (24) are invariant under permutation of the indices, i.e.

$$A_{ijkl}^{s/c} = A_{\mathcal{P}(i)\mathcal{P}(j)\mathcal{P}(k)\mathcal{P}(l)}^{s/c} \quad \mathcal{P} \in \mathcal{S}_4. \quad (25)$$

From this follows that the symmetric group  $\mathcal{S}_4$  is a subgroup of  $G$ . Multiplying all operators  $a_{\mathbf{K},\sigma}^l$  with the same Kagomé index  $l$  by  $-1$  also leaves the Hamiltonian,  $H_{\text{eff}}$ , invariant, because the symbols  $A_{ijkl}^{c/s}$  are nonzero only if the four indices  $ijkl$  are pairwise equal. These two different symmetry operations generate a group with 384 elements. This group  $G$  is isomorphic to the symmetry group of the four-dimensional hypercube. In appendix C the structure of the group  $G$  is discussed and a character table is shown.

To proceed, let  $Q^r$   $r = 0, \dots, 15$  be a basis in the 16 dimensional real vector space,  $V$  of Hermitian  $4 \times 4$  matrices, fulfilling the usual orthonormality and completeness relations

$$Q_{ij}^r Q_{ji}^l = \frac{1}{2} \delta_{rl} \quad \sum_{r=0}^{15} Q_{ij}^r Q_{kl}^r = \frac{1}{2} \delta_{il} \delta_{jk}. \quad (26)$$

This basis can be chosen such, that  $Q^0$  is proportional to the unit matrix,  $Q^{1-3}$  are diagonal,  $Q^{4-9}$  are real and  $Q^{10-15}$  are imaginary. It is convenient to define also the dual matrices

$$K_{ij}^r = \mathcal{F}_{im} \mathcal{F}_{jn} Q_{mn}^r. \quad (27)$$

In TABLE II a choice of a basis  $Q^r$ , which is particularly suitable for our purposes, is shown together with the dual basis  $K^r$ . A representation  $\rho$  of the group  $G$  on  $V$  is given by  $\rho(g)Q^r = N_g^\dagger Q^r N_g$  for  $g \in G$ , where  $N_g$  is the natural four-dimensional representation of  $G$  (cf. appendix C). The representation  $\rho$  is reducible and  $V$  is the direct sum of the four irreducible subspaces  $V^0$ ,  $V^{1-3}$ ,  $V^{4-9}$  and  $V^{10-15}$  spanned by matrices  $Q^0$ ,  $Q^{1-3}$ ,  $Q^{4-9}$  and  $Q^{10-15}$ , respectively. Therefore, the chosen Basis is appropriate for the symmetry group  $G$ . Defining charge and spin density operators

$$\begin{aligned} n_{\mathbf{Q}}^r &= Q_{ij}^r n_{\mathbf{Q}}^{ij} = K_{ij}^r \hat{n}_{\mathbf{Q}}^{ij} \\ \mathbf{S}_{\mathbf{Q}}^r &= Q_{ij}^r \mathbf{S}_{\mathbf{Q}}^{ij} = K_{ij}^r \hat{\mathbf{S}}_{\mathbf{Q}}^{ij}, \end{aligned} \quad (28)$$

the interaction Hamiltonian can be written in a diagonal form as

$$H_{\text{eff}} = \frac{N}{8} \sum_{r=0}^{15} \sum_{\mathbf{Q}} \left( \Lambda_r^s \mathbf{S}_{\mathbf{Q}}^r \mathbf{S}_{-\mathbf{Q}}^r + \frac{1}{4} \Lambda_r^c n_{\mathbf{Q}}^r n_{-\mathbf{Q}}^r \right). \quad (29)$$

The coupling constants  $\Lambda_r^{c/s}$  are equal for all  $Q^r$  belonging to the same irreducible subspace in  $V$ . They are given in TABLE III.

#### V. REDUCTION OF THE SYMMETRY

The tight-binding Hamiltonian in Eq. (11) has a  $U(4)$  symmetry and even after introducing Coulomb interaction, the effective Hamiltonian (29) is invariant under the

$Q^1 (\Gamma_5^a)$	$Q^4 (\Gamma_1^b)$	$Q^7 (\Gamma_5^b)$	$Q^{10} (\Gamma_4)$	$Q^{13} (\Gamma_5^c)$
$\frac{1}{2\sqrt{2}} \begin{pmatrix} 1 & 0 & 0 & 0 \\ 0 & 1 & 0 & 0 \\ 0 & 0 & \bar{1} & 0 \\ 0 & 0 & 0 & \bar{1} \end{pmatrix}$	$\frac{1}{2\sqrt{6}} \begin{pmatrix} 0 & 1 & 1 & 1 \\ 1 & 0 & 1 & 1 \\ 1 & 1 & 0 & 1 \\ 1 & 1 & 1 & 0 \end{pmatrix}$	$\frac{1}{2\sqrt{2}} \begin{pmatrix} 0 & 1 & 0 & 0 \\ 1 & 0 & 0 & 0 \\ 0 & 0 & 0 & \bar{1} \\ 0 & 0 & \bar{1} & 0 \end{pmatrix}$	$\frac{1}{4} \begin{pmatrix} 0 & 0 & \bar{i} & i \\ 0 & 0 & i & \bar{i} \\ i & \bar{i} & 0 & 0 \\ \bar{i} & i & 0 & 0 \end{pmatrix}$	$\frac{1}{4} \begin{pmatrix} 0 & 0 & \bar{i} & \bar{i} \\ 0 & 0 & \bar{i} & \bar{i} \\ i & i & 0 & 0 \\ i & i & 0 & 0 \end{pmatrix}$
$Q^2 (\Gamma_5^a)$	$Q^5 (\Gamma_3)$	$Q^8 (\Gamma_5^b)$	$Q^{11} (\Gamma_4)$	$Q^{14} (\Gamma_5^c)$
$\frac{1}{2\sqrt{2}} \begin{pmatrix} 1 & 0 & 0 & 0 \\ 0 & \bar{1} & 0 & 0 \\ 0 & 0 & 1 & 0 \\ 0 & 0 & 0 & \bar{1} \end{pmatrix}$	$\frac{1}{4} \begin{pmatrix} 0 & 1 & \bar{1} & 0 \\ 1 & 0 & 0 & \bar{1} \\ \bar{1} & 0 & 0 & 1 \\ 0 & \bar{1} & 1 & 0 \end{pmatrix}$	$\frac{1}{2\sqrt{2}} \begin{pmatrix} 0 & 0 & 1 & 0 \\ 0 & 0 & 0 & \bar{1} \\ 1 & 0 & 0 & 0 \\ 0 & \bar{1} & 0 & 0 \end{pmatrix}$	$\frac{1}{4} \begin{pmatrix} 0 & i & 0 & \bar{i} \\ \bar{i} & 0 & i & 0 \\ 0 & \bar{i} & 0 & i \\ i & 0 & \bar{i} & 0 \end{pmatrix}$	$\frac{1}{4} \begin{pmatrix} 0 & \bar{i} & 0 & \bar{i} \\ i & 0 & i & 0 \\ 0 & \bar{i} & 0 & \bar{i} \\ i & 0 & i & 0 \end{pmatrix}$
$Q^3 (\Gamma_5^a)$	$Q^6 (\Gamma_3)$	$Q^9 (\Gamma_5^b)$	$Q^{12} (\Gamma_4)$	$Q^{15} (\Gamma_5^c)$
$\frac{1}{2\sqrt{2}} \begin{pmatrix} 1 & 0 & 0 & 0 \\ 0 & \bar{1} & 0 & 0 \\ 0 & 0 & \bar{1} & 0 \\ 0 & 0 & 0 & 1 \end{pmatrix}$	$\frac{1}{4\sqrt{3}} \begin{pmatrix} 0 & 1 & 1 & \bar{2} \\ 1 & 0 & \bar{2} & 1 \\ 1 & \bar{2} & 0 & 1 \\ \bar{2} & 1 & 1 & 0 \end{pmatrix}$	$\frac{1}{2\sqrt{2}} \begin{pmatrix} 0 & 0 & 0 & 1 \\ 0 & 0 & \bar{1} & 0 \\ 0 & \bar{1} & 0 & 0 \\ 1 & 0 & 0 & 0 \end{pmatrix}$	$\frac{1}{4} \begin{pmatrix} 0 & \bar{i} & i & 0 \\ i & 0 & 0 & \bar{i} \\ \bar{i} & 0 & 0 & i \\ 0 & i & \bar{i} & 0 \end{pmatrix}$	$\frac{1}{4} \begin{pmatrix} 0 & \bar{i} & \bar{i} & 0 \\ i & 0 & 0 & i \\ i & 0 & 0 & i \\ 0 & \bar{i} & \bar{i} & 0 \end{pmatrix}$
$K^1 (\Gamma_5^a)$	$K^4 (\Gamma_1^b)$	$K^7 (\Gamma_5^b)$	$K^{10} (\Gamma_4)$	$K^{13} (\Gamma_5^c)$
$\frac{1}{2\sqrt{2}} \begin{pmatrix} 0 & 1 & 0 & 0 \\ 1 & 0 & 0 & 0 \\ 0 & 0 & 0 & 1 \\ 0 & 0 & 1 & 0 \end{pmatrix}$	$\frac{1}{2\sqrt{6}} \begin{pmatrix} 3 & 0 & 0 & 0 \\ 0 & \bar{1} & 0 & 0 \\ 0 & 0 & \bar{1} & 0 \\ 0 & 0 & 0 & \bar{1} \end{pmatrix}$	$\frac{1}{2\sqrt{2}} \begin{pmatrix} 0 & 1 & 0 & 0 \\ 1 & 0 & 0 & 0 \\ 0 & 0 & 0 & \bar{1} \\ 0 & 0 & \bar{1} & 0 \end{pmatrix}$	$\frac{1}{2} \begin{pmatrix} 0 & 0 & 0 & 0 \\ 0 & 0 & 0 & 0 \\ 0 & 0 & 0 & i \\ 0 & 0 & \bar{i} & 0 \end{pmatrix}$	$\frac{1}{2} \begin{pmatrix} 0 & i & 0 & 0 \\ \bar{i} & 0 & 0 & 0 \\ 0 & 0 & 0 & 0 \\ 0 & 0 & 0 & 0 \end{pmatrix}$
$K^2 (\Gamma_5^a)$	$K^5 (\Gamma_3)$	$K^8 (\Gamma_5^b)$	$K^{11} (\Gamma_4)$	$K^{14} (\Gamma_5^c)$
$\frac{1}{2\sqrt{2}} \begin{pmatrix} 0 & 0 & 1 & 0 \\ 0 & 0 & 0 & 1 \\ 1 & 0 & 0 & 0 \\ 0 & 1 & 0 & 0 \end{pmatrix}$	$\frac{1}{2} \begin{pmatrix} 0 & 0 & 0 & 0 \\ 0 & 1 & 0 & 0 \\ 0 & 0 & \bar{1} & 0 \\ 0 & 0 & 0 & 0 \end{pmatrix}$	$\frac{1}{2\sqrt{2}} \begin{pmatrix} 0 & 0 & 1 & 0 \\ 0 & 0 & 0 & \bar{1} \\ 1 & 0 & 0 & 0 \\ 0 & \bar{1} & 0 & 0 \end{pmatrix}$	$\frac{1}{2} \begin{pmatrix} 0 & 0 & 0 & 0 \\ 0 & 0 & 0 & \bar{i} \\ 0 & 0 & 0 & 0 \\ 0 & i & 0 & 0 \end{pmatrix}$	$\frac{1}{2} \begin{pmatrix} 0 & 0 & i & 0 \\ 0 & 0 & 0 & 0 \\ \bar{i} & 0 & 0 & 0 \\ 0 & 0 & 0 & 0 \end{pmatrix}$
$K^3 (\Gamma_5^a)$	$K^6 (\Gamma_3)$	$K^9 (\Gamma_5^b)$	$K^{12} (\Gamma_4)$	$K^{15} (\Gamma_5^c)$
$\frac{1}{2\sqrt{2}} \begin{pmatrix} 0 & 0 & 0 & 1 \\ 0 & 0 & 1 & 0 \\ 0 & 1 & 0 & 0 \\ 1 & 0 & 0 & 0 \end{pmatrix}$	$\frac{1}{2\sqrt{3}} \begin{pmatrix} 0 & 0 & 0 & 0 \\ 0 & 1 & 0 & 0 \\ 0 & 0 & 1 & 0 \\ 0 & 0 & 0 & \bar{2} \end{pmatrix}$	$\frac{1}{2\sqrt{2}} \begin{pmatrix} 0 & 0 & 0 & 1 \\ 0 & 0 & \bar{1} & 0 \\ 0 & \bar{1} & 0 & 0 \\ 1 & 0 & 0 & 0 \end{pmatrix}$	$\frac{1}{2} \begin{pmatrix} 0 & 0 & 0 & 0 \\ 0 & 0 & i & 0 \\ 0 & \bar{i} & 0 & 0 \\ 0 & 0 & 0 & 0 \end{pmatrix}$	$\frac{1}{2} \begin{pmatrix} 0 & 0 & 0 & i \\ 0 & 0 & 0 & 0 \\ 0 & 0 & 0 & 0 \\ \bar{i} & 0 & 0 & 0 \end{pmatrix}$

TABLE II: The matrices  $Q^{1-15}$  are a choice of an orthonormal complete basis of the 15 dimensional real vector space of traceless hermitian matrices, so called generators of  $SU(4)$ , that is adequate to the symmetry of the  $\text{CoO}_2$ -layer. The matrices  $K^r$  are obtained from  $Q^r$  by Eq. (27). Note that  $\bar{1} = -1$  and  $\bar{i} = -i$ .  $2\sqrt{2}Q^0 = 2\sqrt{2}K^0$  is the  $4 \times 4$  unit matrix.

$r$	0	1-3	4-9	10-15
$\Lambda_r^c$	$\frac{2}{9}(3U + 12U' - 6J_H)$	$\frac{2}{9}(3U - 4U' + 2J_H)$	$\frac{2}{9}(-2U' + 4J_H - 2J')$	$\frac{2}{9}(-2U' + 4J_H + 2J')$
$\Lambda_r^s$	$-\frac{2}{9}(3U + 6J_H)$	$-\frac{2}{9}(3U - 2J_H)$	$-\frac{2}{9}(2U' - 2J')$	$-\frac{2}{9}(2U' + 2J')$

TABLE III: The coefficients  $\Lambda_r^{s/c}$ .

symmetry group  $G$ . In a real  $\text{CoO}_2$  plane this symmetry is reduced even in the paramagnetic state. There are terms in the Hamiltonian of the real system that restrict the symmetry operations of  $G$  to the subgroup, which describes real crystallographic space-group symmetries.

A trigonal distortion of the oxygen octahedra by approaching the two O-layers to the Co-layer, is for example compatible with the point group symmetry  $D_{3d}$  of the  $\text{CoO}_2$  layer. However it lifts the degeneracy of the

$t_{2g}$ -orbitals, leading to a term

$$\begin{aligned} H_{\text{tr}} &= D_{\text{tr}} \sum_{k\sigma} \sum_{m \neq m'} c_{km\sigma}^\dagger c_{km'\sigma} \\ &= D_{\text{tr}} \sum_{l\kappa\sigma} \sum_{m \neq m'} b_{l\kappa m\sigma}^\dagger b_{l\kappa m'\sigma} e^{i\mathbf{B}_l \cdot (\mathbf{a}_m - \mathbf{a}_{m'})} \end{aligned} \quad (30)$$

in the Hamiltonian, where we used Eq. (8) to obtain the second line. For the top band we obtain with Eq. (16) and (B4)

$$\begin{aligned} H_{\text{tr}} &= \sqrt{2/3} D_{\text{tr}} 4 \sum_{l\kappa\sigma} (K_{ll}^4 + O(\kappa^2)) b_{l\kappa\sigma}^\dagger b_{l\kappa\sigma} \\ &\approx \sqrt{2/3} D_{\text{tr}} N n_0^4 \end{aligned} \quad (31)$$

where the matrix  $K^4$  is given in TABLE II and  $\kappa = |\mathbf{k}|a$  is small for the relevant states near the Fermi pockets, if the pockets are small enough. Similarly, a finite direct hopping integral  $t_{dd}$  leads to the term

$$\begin{aligned} H_{dd} &= t_{dd} \sum_{km\sigma} 2 \cos(k_m) c_{km\sigma}^\dagger c_{km\sigma} \\ &= 4\sqrt{6}t_{dd} \sum_{l\kappa\sigma} (K_{ll}^4 + O(\kappa^2)) b_{l\kappa\sigma}^\dagger b_{l\kappa\sigma} \\ &\approx \sqrt{6}t_{dd} N n_0^4 \end{aligned} \quad (32)$$

where we again dropped the terms involving the lower bands in the second line. In fact, any other additional hopping term or any quadratic perturbation compatible with the space group is proportional to the field  $n_0^4$  in the limit of small pockets, if the perturbation is diagonal in the spin indices. As the trigonal distortion of the octahedra is nonzero and additional hopping terms are present in the CoO<sub>2</sub>-layer, a term proportional to  $n_0^4$  exists in the Hamiltonian acting like a symmetry breaking field. For simplicity, we will refer to a term proportional to  $n_0^4$  in the Hamiltonian as the *trigonal distortion*, even though this term is rather an effective trigonal distortion that also includes the effects of additional hopping terms.

From the matrix  $K^4$  can be seen, that the presence of a finite field,  $n_0^4$ , in the Hamiltonian leads to a distinction between the  $\Gamma$  and the M points in the BZ and the four hole pockets are no longer equivalent. In real space, the four Kagomé lattices are still equivalent, as they transform under space group symmetries among themselves. In fact, the matrix  $Q^4$  is still invariant under permutations of rows and columns, i.e.  $N_g^T Q^4 N_g = Q^4$  for all  $g \in \mathcal{S}_4$ , but  $Q^4$  is not invariant under changing the sign of all operators with the same Kagomé index. These sign changes, however, are not space-group symmetries, but gauge symmetries, originating from the fact that the charge on the Kagomé lattices is conserved by  $H_{\text{tb}}$  and also by the Coulomb interaction except for the pair-hopping term proportional to  $J'$  in Eq. (15). This term however can only change the number of electrons by two, leading to these gauge symmetries, that are broken, as soon as single electron hopping processes between the Kagomé lattices are introduced.

To classify the states according to the real symmetry group of the CoO<sub>2</sub>-layer without gauge symmetries, it is therefore sufficient, to consider the presence of a small field  $n_0^4$ , that restricts the symmetry group  $G$  to a subgroup, consisting of space group symmetries of the CoO<sub>2</sub>-layer. This subgroup of  $G$  is isomorphic to  $\mathcal{S}_4 \simeq T_d \simeq O$ . Intuitively it is understandable that the symmetry of the four dimensional cube reduces to the symmetry of a three dimensional cube, if one of the four hole pockets is not equivalent to the other three.

From TABLE II can be seen, that the matrices  $Q^0$ ,  $Q^{1-3}$ ,  $Q^4$ ,  $Q^{5-6}$ ,  $Q^{7-9}$ ,  $Q^{10-12}$  and  $Q^{13-15}$  transform irreducibly under  $\mathcal{S}_4$  with the representations  $\Gamma_1^a$ ,  $\Gamma_5^a$ ,  $\Gamma_1^b$ ,  $\Gamma_3$ ,  $\Gamma_5^b$ ,  $\Gamma_4$  and  $\Gamma_5^c$ , respectively, where the upper-script letter distinguishes between different subspaces transforming with the same representation.

The appearance of three dimensional irreducible representations in the classification of the order parameters can be understood as follows. The point group  $P$  of a single CoO<sub>2</sub>-layer is  $D_{3d}$ , and the degree of its irreducible representations is  $\leq 2$ . The point group is the factor group  $S/T$  where  $S$  is the space group of the CoO<sub>2</sub>-layer and  $T$  is the subgroup of all pure translations. For our system it is convenient to consider the factor group  $P' = S/2T$ , where  $2T$  is the subgroup of  $T$  that is generated by translations of  $2\mathbf{a}_i$ .  $P'$  is isomorphic to the cubic group  $O_h$  and has irreducible representations of degree 3. The operators  $n_{\mathbf{Q}}^r$  and  $\mathbf{S}_{\mathbf{Q}}^r$  transforms irreducibly under the translations in  $2T$  for every  $r$ . The symmetry operations of  $P'$  however mix operators  $n_{\mathbf{Q}}^r$  (or  $\mathbf{S}_{\mathbf{Q}}^r$ ) with different  $r$ , and the irreducible representations as given above or shown in TABLE II are obtained. Strictly speaking, the basis of SU(4) generators shown in TABLE II is the correct eigenbasis only for an infinitesimal small trigonal distortion, for a finite distortion, the representations  $\Gamma_1^a$  and  $\Gamma_1^b$  as well as  $\Gamma_5^a$  and  $\Gamma_5^b$  can hybridize as they transform with the same irreducible representation. Note, that  $\Gamma_5^c$  transforms differently under time reversal. The situation here is similar to atomic physics, where a crossover from the Zeeman effect to the Paschen-Back effect with increasing magnetic field occurs, because states with the same  $J_z$  can hybridize.

## VI. ORDERING PATTERNS

In this section the different types of symmetry breaking phase transitions are discussed in a mean-field picture. The symmetry breaking is due to existence of a finite order parameter, that is in our case given by the expectation value  $\langle n_{\mathbf{Q}}^r \rangle$  of  $\langle \mathbf{S}_{\mathbf{Q}}^r \rangle$ . Note, that a finite expectation value  $\langle n_0^0 \rangle$  or  $\langle n_0^4 \rangle$  does not break any symmetry of the CoO<sub>2</sub>-layer.

In our tight-binding model as it was discussed in section II, the susceptibility,  $\chi^0$  is given by 4 identical plateaux around the  $\Gamma$  and the M points. In the presence of a trigonal distortion, the susceptibility still keeps a plateaux like structure but the diameter of the plateaux

decreases, such that the susceptibility appears sharply enhanced around the M and the  $\Gamma$  points. Therefore we restrict the discussion to the case where  $\mathbf{Q}$  equals zero and write  $n^r$  and  $\mathbf{S}^r$  instead of  $n_{\mathbf{0}}^r$  and  $\mathbf{S}_{\mathbf{0}}^r$  from now on. Note, that in our formalism the states with  $\mathbf{Q} = 0$  describe periodic states with the enlarged unitcell of the Kagomé lattice. But the internal degrees of freedom within this enlarged unitcell still allows for rather complicated charge- and spin-patterns. States with a small but finite  $\mathbf{Q}$  describe modulations of these local states on long wavelengths. It is therefore important to understand first the local states the are described by  $\mathbf{Q} = 0$  instabilities. Furthermore, only  $\mathbf{Q} = 0$  states couple to the periodic potential produced by a Na superstructure at  $x = 0.5$ .

The  $\mathbf{Q} = 0$  instabilities lead to a chemical potential difference for states belonging to different hole pockets. In general, the BZ is folded and states of different hole pockets combine to new quasi-particles. In this case, translational and/or rotational symmetry is broken. Complex ordering patterns can be realized without opening of gaps, i.e. the system stays metallic.

We consider first the orderings given by a finite expectation value of the charge density operators  $n^r$ . This expectation value is given by

$$\langle n^r \rangle = \frac{4}{N} \sum_{\mathbf{k}\sigma} \lambda_l^r \langle v_{\mathbf{k}\sigma}^\dagger v_{\mathbf{k}\sigma}^l \rangle, \quad (33)$$

where  $\lambda_l^r$  are the eigenvalues of the matrix  $Q^r$  ( $U_{ki}^r Q_{ij}^r U_{lj}^r = \lambda_l^r \delta_{kl}$ ) and  $v_{\mathbf{k}\sigma}^l = U_{ln}^r a_{\mathbf{k}\sigma}^n$  are the creation operators of the quasi-particles. If only one  $\langle n^r \rangle \neq 0$ , the effective interaction Hamiltonian in the mean-field approximation reduces to

$$\frac{\Lambda_r^c \langle n^r \rangle}{4} \sum_{\mathbf{k}\sigma} \lambda_l^r v_{\mathbf{k}\sigma}^\dagger v_{\mathbf{k}\sigma}^l. \quad (34)$$

If the coupling constant  $\Lambda_r^c$  is negative, the interaction energy of the system can be lowered by introducing an imbalance between the occupation numbers  $n_l = \sum_{\mathbf{k}\sigma} \langle v_{\mathbf{k}\sigma}^\dagger v_{\mathbf{k}\sigma}^l \rangle$ . The operators  $v_{\mathbf{k}\sigma}^\dagger$  create Bloch states with momentum  $\mathbf{k}$  in the reduced BZ. The amplitudes of the three  $t_{2g}$  orbitals on a given Co site with these Bloch states can be obtained from Eq. (6) and (7) and the relation  $a_{\mathbf{k}}^\dagger \approx 1/\sqrt{3} \sum_m a_{\mathbf{k}m}^\dagger$  which follows from Eq. (9) and (16).

For the matrices  $Q^{0-4}$ , these Bloch states are given by a single  $t_{2g}$  orbital on each Co site. For the non-diagonal matrices  $Q^{4-9}$  these Bloch states are on each Co site proportional to a linear combination of  $t_{2g}$  orbitals of the form

$$\frac{1}{\sqrt{3}} (s_x d_x + s_y d_y + s_z d_z) \quad \text{with } s_x, s_y, s_z \in \{\pm 1\}. \quad (35)$$

This linear combination is the atomic  $d$ -orbital  $\varphi_0 \equiv \mathcal{Y}_{20}$  parallel to the body-diagonal  $[s_x, s_y, s_z]$  of the cubic unitcell around a Co atom.

The eigenvectors of the of the matrices  $Q^{10-15}$  are complex. A complex linear combination of  $t_{2g}$  orbitals has in general a non-vanishing expectation value of the orbital angular momentum operator  $\mathbf{L}$ . In TABLE IV the angular momentum expectation values, which are relevant for our discussion are shown.

$(id_x + d_y + d_z)/\sqrt{3}$	$\langle \mathbf{L} \rangle = \hbar(0, -1, 1)2/3$ (cyclic)
$(id_x + d_y - d_z)/\sqrt{3}$	$\langle \mathbf{L} \rangle = \hbar(0, 1, 1)2/3$ (cyclic)
$(d_x + \omega^2 d_y + \omega d_z)/\sqrt{3}$	$\langle \mathbf{L} \rangle = \hbar(1, 1, 1)/\sqrt{3}$
$(\omega^2 d_y + \omega d_z)/\sqrt{2}$	$\langle \mathbf{L} \rangle = \hbar(1, 0, 0)\sqrt{3}/2$ (cyclic)

TABLE IV: The expectation values the angular momentum operator  $\mathbf{L}$  for several complex linear combinations of  $t_{2g}$  orbitals.  $\omega = e^{2\pi i/3}$

The quasi-particles  $v_{\mathbf{k}\sigma}^l$  are expressed in terms of pocket operators by  $v_{\mathbf{k}\sigma}^l = \hat{U}_{lm}^r b_{\mathbf{k}\sigma}^m$ , where the unitary matrix  $\hat{U}_{lm}^r = U_{ln}^r \mathcal{F}_{nm}$  diagonalizes  $K^r$ . From this follows that if  $K^r$  is already diagonal, no folding of the BZ occurs and translational symmetry is not broken. Otherwise, the BZ is folded and states of different pockets recombine to form the new quasi-particles.

Now we consider finite expectation values of the spin-density operators  $\mathbf{S}^r$ . Due to the absence of spin-orbit coupling, our model has an  $SU(2)$  rotational symmetry in spin space. Therefore the discussion can be restricted to the order parameters  $\langle S_z^r \rangle = \langle \mathbf{e}_z \cdot \mathbf{S}^r \rangle$ , given by

$$\langle S_z^r \rangle = \frac{2}{N} \sum_{\mathbf{k}\sigma} \lambda_l^r \sigma \langle v_{\mathbf{k}\sigma}^\dagger v_{\mathbf{k}\sigma}^l \rangle, \quad (36)$$

where  $\sigma$  takes the values 1 and  $-1$  corresponding to spin up and down. If only one  $\langle S_z^r \rangle \neq 0$ , the effective interaction Hamiltonian reduces to

$$\frac{\Lambda_r^s \langle S_z^r \rangle}{2} \sum_{\mathbf{k}\sigma} \lambda_l^r \sigma v_{\mathbf{k}\sigma}^\dagger v_{\mathbf{k}\sigma}^l. \quad (37)$$

The mean-field Hamiltonian (37) is given by the same quasi-particles and the same eigenvalues  $\lambda_l^r$  as the Hamiltonian in (34). The only difference is that the sign of the splitting of the quasi-particle bands depends on the spin. In the following, all ordering transitions with order parameters  $\langle n^r \rangle$  and  $\langle S_z^r \rangle$  for  $r = 0, \dots, 15$  are shortly discussed.

**r=0**

*charge:*  $\langle n^0 \rangle$  is the total charge of the system, which is fixed and non-zero, even in the paramagnetic phase.

*spin:* A finite  $\langle S_z^0 \rangle$  describes a Stoner ferromagnetic instability. The coupling constant  $\Lambda_0^s$  given in TABLE III is the most negative coupling constant. In the unperturbed system without trigonal distortion, the critical temperature of all continuous transitions discussed here,

only depends on the density of states and on the coupling constant in the mean-field picture. In this case, ferromagnetism is the leading instability for the unperturbed system. In the real  $\text{CoO}_2$ -plane, this must not necessarily occur, but strong ferromagnetic fluctuations will be present in any case.

$$\mathbf{r}=1-3$$

*charge:* A finite expectation value  $\langle n^r \rangle$  for  $r = 1, 2, 3$  corresponds to a difference in the charge density on the four Kagomé lattices, because the matrices  $Q^{1-3}$  of TABLE II are diagonal and the quasi-particles  $v_{\mathbf{k}\sigma}^\dagger$  are just the Kagomé states  $a_{\mathbf{k}\sigma}^\dagger$ . From the view point of Fermi surface pockets given by  $K^{1-3}$  which are non-diagonal, this order yields a folding of the BZ, because the quasi-particles  $v_{\mathbf{k}\sigma}^\dagger$  are linear combinations of states belonging to different hole pockets. This means that the translational symmetry is broken. In the matrix  $Q^{1-3}$  we find two positive and two negative diagonal elements. Consequently, a finite expectation value  $\langle n^{1-3} \rangle$  leads to a charge enhancement on two Kagomé lattices and to a charge reduction on the other two. As specifying two Kagomé lattices specifies a direction on the triangular lattice, rotational symmetry is broken and crystal symmetry is reduced from hexagonal to orthorhombic. The phases described by the matrices  $Q^{1-3}$  have the same coupling constant  $\Lambda_1^c$  because they transform irreducibly into each other under crystal symmetries with the representation  $\Gamma_5^g$ . In order to examine which linear combinations of the three order parameters  $\langle n^1 \rangle$ ,  $\langle n^2 \rangle$  and  $\langle n^3 \rangle$  could be stable below the critical temperature, we consider the Landau expansion of the free energy  $\Delta F = F - F_0$

$$\Delta F = \frac{\alpha}{2}(\eta_1^2 + \eta_2^2 + \eta_3^2) + \beta \eta_1 \eta_2 \eta_3 + \frac{\gamma_1}{4}(\eta_1^2 + \eta_2^2 + \eta_3^2)^2 + \frac{\gamma_2}{4}(\eta_1^2 \eta_2^2 + \eta_2^2 \eta_3^2 + \eta_3^2 \eta_1^2), \quad (38)$$

with  $\eta_1 = \langle n^1 \rangle$ ,  $\eta_2 = \langle n^2 \rangle$ ,  $\eta_3 = \langle n^3 \rangle$ . For  $\gamma_1 > \max\{0, -\gamma_2\}$ , the free energy is globally stable. For  $\gamma_2 < 0$ , Eq. (38) has a minimum of the form  $\eta_1 = \eta_2 = \eta_3$ , if  $\beta^2 - 4\alpha(3\gamma_1 + \gamma_2) > 0$ . This phase is described by the symmetric combination  $\tilde{Q}^1 = (Q^1 + Q^2 + Q^3)/\sqrt{3}$  which does not break the rotational symmetry. In FIG. 3, the folding of BZ and the splitting of the bands (the dotted line is triply degenerate) and the orbital pattern of the quasi-particles  $v_{\mathbf{k}\sigma}^\dagger = a_{\mathbf{k}\sigma}^\dagger$  are shown. Note that  $\tilde{Q}^1$  has one positive and three negative diagonal elements. The charge is enhanced or reduced on a single Kagomé lattice depending on the sign of the coefficient  $\beta$  in Eq. (38). The third-order term in the free energy expansion is allowed by symmetry, because there is no inversion-like symmetry that would switch the of  $(\eta_1, \eta_2, \eta_3) \rightarrow (-\eta_1, -\eta_2, -\eta_3)$ . Therefore the transition can be first order. On the other hand, for  $\gamma_2 > 0$ , there is a competition between the

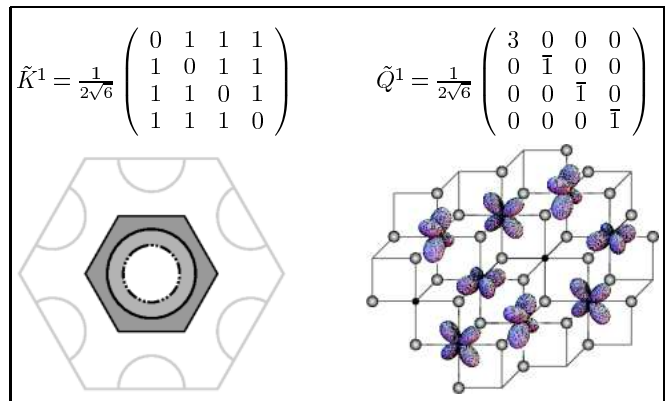


FIG. 3: Charge ordering instability with finite expectation value  $\langle \tilde{n}_0^1 \rangle$  leading to a charge enhancement or reduction on one Kagomé lattice. The folding of the BZ and the splitting of the pockets is shown (The double dotted line in the BZ indicates a triply degenerate pocket). On the right a quasi-particle state that is in this case just a Kagomé lattice state is drawn.

terms proportional to  $\gamma_2$  and  $\beta$  in Eq. (38). The minimum has not a simple form. For  $|\beta| \ll \gamma_2$ , however, the transition yields states approximately described by the matrix  $Q^1$ ,  $Q^2$  or  $Q^3$ . In any case this phase does break the rotational symmetry.

*spin:* The spin density mean-fields  $\langle S_z^i \rangle$   $i = 1, 2, 3$  transform under space group symmetries like  $\Gamma_5^g$  and time reversal symmetry gives  $\langle S_z^i \rangle$  to  $-\langle S_z^i \rangle$ . Due to the latter the third order term in Eq. (38) is forbidden, so that the transition is continuous. For  $\gamma_2 < 0$ , Eq. (38) has again a minimum of the form  $\eta_1 = \eta_2 = \eta_3$ , whereas for  $\gamma_2 > 0$  the minimum is realized for  $\eta_1 \neq 0$  and  $\eta_2 = \eta_3 = 0$  (and permutations), if  $\alpha < 0$ . The folding of the BZ, the quasi-particles and the breaking of space-group symmetries is the same as for the charge density operators  $n^i$ . However, the splitting of the bands depends now on the spin and time reversal symmetry is broken.

These states are spin density waves, spatial modulations of the spin density with a vanishing total magnetization. The two different types of spin density modulations for  $\gamma_2 > 0$  or  $\gamma_2 < 0$  are shown in Fig. 4. For  $\gamma_2 > 0$  rotational and translational symmetry is broken yielding a collinear spin orientation along one spatial direction and alternation perpendicular. In contrast  $\gamma_2 < 0$  yields a rotationally symmetric spin density wave with a doubled unit cell. This special type of spin density wave gives a subset of lattice points, forming a triangular lattice, of large spin density and another subset with opposite spin density of a third in size, forming a Kagomé lattice. Both states are metallic, because no gaps are opened at the FS. This spin density wave is not a result of Fermi surface nesting, but due to the complex orbital structure. The coupling constant for this transition,  $\Lambda_1^s$  is the second strongest coupling in the model Hamiltonian after the ferromagnetic coupling constant,  $\Lambda_0^s$ , as it is best seen in Fig. 7.

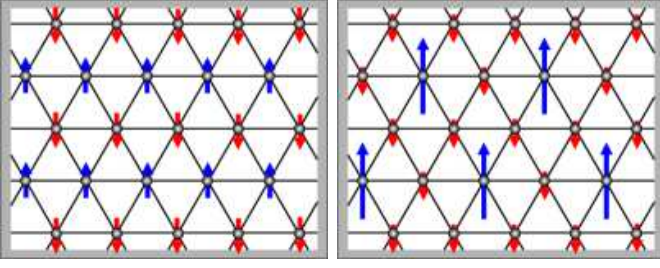


FIG. 4: The spin density wave patterns corresponding to a finite expectation value  $\langle S_z^1 \rangle$  is shown on the left. This pattern is stabilized if  $\gamma_2 > 0$  in Eq. (38). The pattern on the right corresponds to a finite order parameter  $\langle S_z^1 + S_z^2 + S_z^3 \rangle$ , which is stabilized for  $\gamma_2 < 0$ .

$\mathbf{r}=4$

*charge:* As discussed in section V, a finite expectation value of  $n^4$  does not break any space group symmetry. The matrix  $K^4$  is diagonal with one positive and three negative elements. This leads to a change of the band energy of the band at the  $\Gamma$  point relative to those at the  $M$  points (Fig. 5a)). This results in an orbital order, a pattern as shown in Fig. 5a), because the number of holes associated with the hole pocket around the  $\Gamma$ -point is different from that of the other pockets. The net charge onsite vanishes, but the charge distribution has the quadrupolar form, which results from

$$\begin{aligned} \rho(r) &\propto \frac{1}{4} [3|\psi_{yz} + \psi_{zx} + \psi_{xy}|^2 - |\psi_{yz} - \psi_{zx} + \psi_{xy}|^2 \\ &\quad - |\psi_{yz} + \psi_{zx} - \psi_{xy}|^2 - |\psi_{yz} - \psi_{zx} - \psi_{xy}|^2] \\ &= \psi_{yz}^* \psi_{zx} + \psi_{zx}^* \psi_{xy} + \psi_{xy}^* \psi_{yz} + c.c. . \end{aligned} \quad (39)$$

The corresponding tensor operator belongs to the representation  $\Gamma_1$  of the subgroup  $D_3$  of the cubic group with the three-fold rotation axis parallel to  $[111]$ , i.e. along the  $c$ -axis perpendicular to layer. This quadrupolar field would be driven by the symmetry reduction discussed above, through trigonal distortion and direct  $dd$ -hopping among the  $t_{2g}$ -orbitals.

*spin:* While the corresponding order parameter  $\langle S_z^4 \rangle$  breaks time reversal symmetry, space group symmetry is conserved. This order is spatially uniform analogous to a ferromagnet without, however, having a net magnetic moment. Because the magnetic moment associated with the Fermi surface pocket at the  $\Gamma$ -point is opposite and three times larger than the moment at the three  $M$ -pockets. While the net dipole moment vanishes on every site, this configuration has a finite quadrupolar spin density corresponding to the onsite spin density distribution of the same form as the charge distribution in Eq.(39), which also belongs to  $\Gamma_1$  representation of  $D_3$ . It is also important to note that no third order terms are allowed due to broken time reversal symmetry, such that the transition to this order would be continuous.

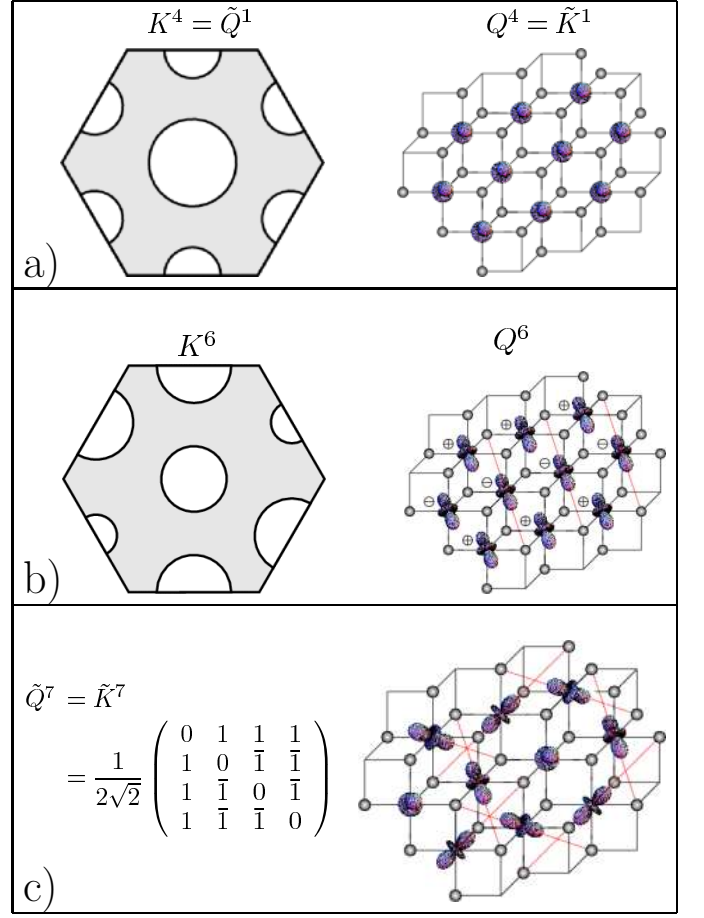


FIG. 5: Ordering instabilities, described by real off-diagonal  $SU(4)$  generators  $Q^{4-9}$ . a)  $Q^4$  breaks neither translational nor rotational symmetry. b) shows the ordering corresponding to  $Q^6$ . The ordering shown in c) is described in real space and in reciprocal space by the same matrix  $\tilde{Q}^7 = \tilde{K}^7$  and breaks translational symmetry. The corresponding BZ is shown in FIG. 3.

$\mathbf{r}=5,6$

*charge:* The order parameters  $\langle n^5 \rangle = \eta_5$  and  $\langle n^6 \rangle = \eta_6$  transform according to the irreducible representation  $\Gamma_3$  of the cubic point group. The Landau expansion of the free energy is given by

$$\Delta F = \frac{\alpha}{2}(\eta_5^2 + \eta_6^2) + \frac{\beta}{3}\eta_6(3\eta_5^2 - \eta_6^2) + \frac{\gamma}{4}(\eta_5^2 + \eta_6^2)^2, \quad (40)$$

whose global stability requires  $\gamma > 0$ . The third order term, allowed here, induces a first order transition and simultaneously introduce an anisotropy which is not present in the second- and fourth-order terms. We can write  $(\eta_5, \eta_6) = \eta(\cos \varphi, \sin \varphi)$  and obtain

$$\Delta F = \frac{\alpha}{2}\eta^2 + \frac{\beta}{3}\eta^3 \sin 3\varphi + \frac{\gamma}{4}\eta^4 \quad (41)$$

Depending on the sign of  $\beta$  the stable angles will be  $\varphi = \sin(\beta)\pi/2 + 2\pi n/3$ . This yields three degenerate states

of uniform orbital order whose charge distribution has the quadrupolar form:

$$\rho(r) \propto e^{i\varphi} \{(\psi_{zx}^* \psi_{xy} + \psi_{xy}^* \psi_{zx}) + \omega(\psi_{yz}^* \psi_{zx} + \psi_{zx}^* \psi_{yz}) + \omega^2(\psi_{xy}^* \psi_{yz} + \psi_{yz}^* \psi_{xy})\} + c.c. \quad (42)$$

with a tensor operator belonging to  $\Gamma_3$  of  $D_3$ . Each state is connected with the choice of one  $M$ -pocket which has a different filling compared to the other two (Fig. 5b). The main axis of each state points locally along one of the three cubic body-diagonals,  $[\bar{1}, 1, 1]$ ,  $[1, \bar{1}, 1]$ ,  $[1, 1, \bar{1}]$ , and the sign of the local orbital wave function is staggered along the corresponding direction on the triangular lattice,  $[\bar{2}, 1, 1]$ ,  $[1, \bar{2}, 1]$ ,  $[1, 1, \bar{2}]$ . In this way the rotational symmetry is broken but the translational symmetry is conserved. The matrices  $Q^5$  and  $Q^6$  commute with  $Q^4$  such that the external symmetry reduction has only a small effect on this type of order.

*spin*: The spin densities  $\langle S_z^5 \rangle$  and  $\langle S_z^6 \rangle$  also belong to the two-dimensional representation  $\Gamma_3$  of the cubic point group. Here time reversal symmetry ensures that the Landau expansion only allows even orders of the order parameter  $(\eta_5, \eta_6) = \eta(\cos \varphi, \sin \varphi)$  (i.e.  $\beta = 0$  in Eq.(40)). The continuous degeneracy in  $\varphi$  is only lifted by the sixth order term, given by

$$\frac{\delta_1}{6}(\eta_1^2 + \eta_2^2)^3 + \frac{\delta_2}{6}\eta_2^2(3\eta_1^2 - \eta_2^2)^2 = \frac{\delta_1}{6}\eta^6 + \frac{\delta_2}{6}\eta^2 \sin^2 3\varphi \quad (43)$$

Stability requires  $\delta_1 > \max\{0, -\delta_2\}$ . The anisotropy is lifted by the  $\delta_2$ -term which give rise to two possible sets of three-fold degenerate states. Depending on the sign of  $\delta_2$  we have a minimum of the free energy for  $\varphi = (1 - \text{sign}\delta_2)\pi/4 + \pi n$ . The corresponding spin densities have no net dipole on every site, but again a quadrupolar form of the same symmetry as for the charge, given by Eq.(42).

### r=7-9

*charge*: The order parameters  $\langle n^i \rangle$  for  $i = 7, 8, 9$  transform irreducibly under space group symmetries with the representation  $\Gamma_5^b$ . The expansion (38) of the free energy holds also for these order parameters. The third order term makes the transition first order and favors the symmetric rotationally invariant combination of the order parameters, described by the matrix  $\tilde{Q}^7 = (Q^7 + Q^8 + Q^9)/\sqrt{3} = \tilde{K}^7$  shown in FIG. 5c). The folding of the BZ and the splitting of the bands is the same as in Fig. 3. The orbital pattern of the non-degenerate quasi-particle band is also shown in Fig. 5c). It consists of atomic  $\varphi^0$  orbitals pointing along all four cubic space diagonals. Translational but not rotational symmetry is broken.

*spin*: The discussion for the spin density operators is analogous to the discussion in the section **r = 1 - 3**.

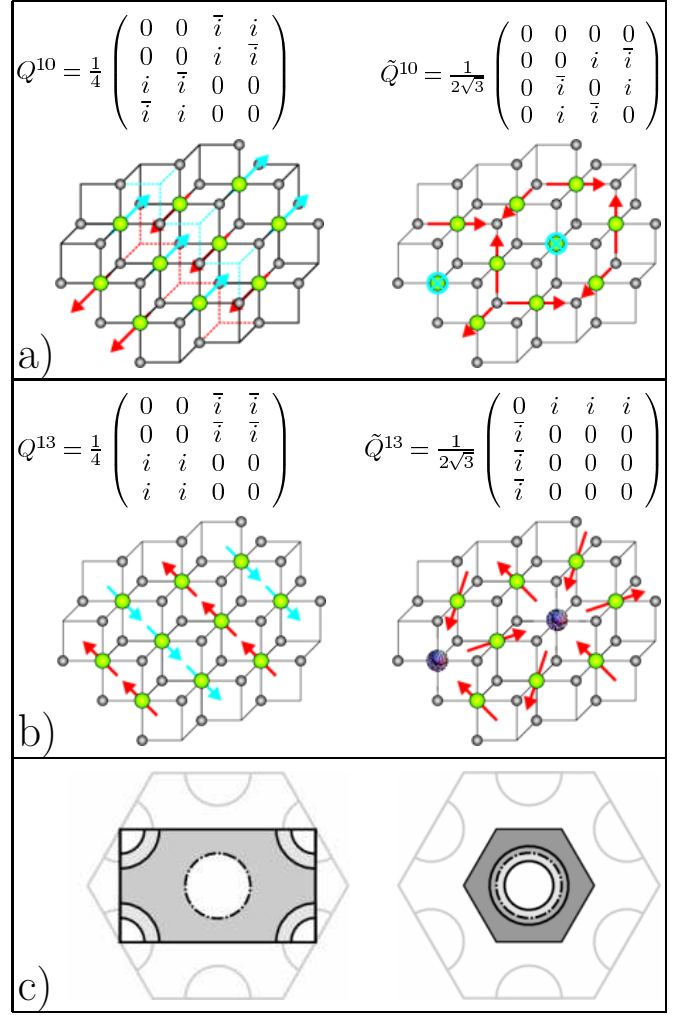


FIG. 6: Transitions to time reversal symmetry breaking states, where the expectation value of the orbital angular momentum  $\langle \tilde{L} \rangle$  on the Co-sites is finite. a) States where the angular momentum does not lie in the plane.  $\tilde{K}^{10} = \tilde{Q}^{10}$  b) States with angular momentum in the plane.  $\tilde{K}^{13} = -\tilde{Q}^{13}$ . c) The folding of the BZ and the hybridization of the bands for a) are shown. Dotted lines indicate double degenerate bands.

### r=10-12

*charge*: The order parameters  $\langle n^i \rangle$  for  $i = 10, 11, 12$  transform irreducibly under space group symmetries with the representation  $\Gamma_4$ . For the  $\Gamma_4$  representation of  $T_d$ , there is no third order invariant. All other terms in Eq. (38) are however also invariants for  $\Gamma_4$ . The absence of the third order term leads to continuous transition. The stabilized state for  $\alpha < 0$  depends on the sign of  $\gamma_2$  in Eq. (38).

For  $\gamma_2 > 0$  a nontrivial minimum with  $\langle n^{11} \rangle = \langle n^{12} \rangle = 0$  exists, which is described by the hermitian, imaginary matrix  $Q^{10}$ . If  $\lambda$  is an eigenvalue of  $Q^{10}$ , then  $-\lambda$  is also an eigenvalue of  $Q^{10}$  and the corresponding quasi-particles are connected by time reversal symmetry.

Therefore the non-vanishing eigenvalues of  $Q^{10}$  belong to quasi-particle states, which are not invariant under time reversal symmetry. They are given by complex linear combinations of  $t_{2g}$  orbitals. For complex linear combinations of  $t_{2g}$  orbitals, the expectation value of the orbital angular momentum operator  $\langle \mathbf{L} \rangle$  does not vanish in general, as can be seen from TABLE IV. In FIG. 6a), the pattern of the angular momentum expectation values  $\langle \mathbf{L} \rangle$  for a quasi-particle of  $Q^{10}$  is shown. It is invariant under translations along  $\mathbf{a}_1$  and staggered under translations along  $\mathbf{a}_2$  and  $\mathbf{a}_3$ . The expectation values are parallel to [011]. The folding of the BZ and the splitting of the bands is shown in Fig. 6c). Rotational, translational and time reversal symmetry is broken and the state has the magnetic point-group  $\underline{2}/m$ .

For  $\gamma_2 < 0$  the symmetric combination  $\tilde{Q}^{10} = (Q^{10} + Q^{11} + Q^{12})/\sqrt{3} = \tilde{K}^{10}$  is stabilized. The angular momentum pattern for a quasi-particle with non-vanishing eigenvalue is shown in FIG. 6a). Depending on the site, the expectation value points along [100], [010], [001] or  $[\bar{1}\bar{1}\bar{1}]$  and the magnitudes are such, that the pattern is rotationally invariant and the expectation value of the total angular momentum perpendicular to the plane vanishes. The folding of the BZ and the splitting of the pockets is shown in FIG. 6c). This state has the magnetic point group  $\underline{3}m$ . Note, that these states can also be considered as a kind of staggered flux states. The matrices  $Q^{10-12}$  commute with  $Q^4$  and therefore the transitions are only little affected by a trigonal distortion.

*spin:* The spin density order parameters  $\langle S_z^i \rangle$  for  $i = 10, 11, 12$  also transform under space group symmetries like  $\Gamma_4$  and except for the spin dependent quasi-particle energy, the discussion is the same as for the charge density operators. Note, however, that these spin density operators do not change sign under time reversal symmetry, because both the orbital angular momentum and the spin is reversed. This, however does not lead to a third order term in the Landau expansion, as there is no third order invariant for the  $\Gamma_4$  representation anyway.

### r=13-15

*charge:* The order parameters  $\langle n^i \rangle$  for  $i = 13, 14, 15$  transform irreducibly under space group symmetries with the representation  $\Gamma_5^c$ . The matrices  $Q^{13-15}$  are also imaginary and time reversal symmetry changes the sign of the order parameters. The Landau expansion of the free energy is given as above by Eq. (38) with  $\beta = 0$ .

For  $\gamma_2 > 0$  and  $\alpha < 0$  a minimum of the free energy is given by the order parameter  $\langle n^{13} \rangle$ . The angular momentum pattern of the quasi-particles is shown in FIG. 6b). The expectation values lie in the  $\text{CoO}_2$ -plane and are parallel to the  $\mathbf{a}_1$  direction. Their sign is staggered along the  $\mathbf{a}_2$  and  $\mathbf{a}_3$  direction. The quasi-particles consist of states belonging to the  $\Gamma$  and the M pocket. The folding of the BZ is given in FIG. 6c), but with the single dotted line in the center being a doubly degenerate M pocket.

Rotational, translational and time reversal symmetry is broken.

For  $\gamma_2 < 0$  the symmetric combination  $\tilde{Q}^{13} = (Q^{13} + Q^{14} + Q^{15})/\sqrt{3} = -\tilde{K}^{13}$  is stabilized. The pattern of the quasi-particles corresponding to  $\tilde{Q}^{13}$  is shown in FIG. 6b). It consists of non-magnetic sites with a  $\varphi_0$  orbital perpendicular to the plane and of sites with angular momentum expectation values along  $\mathbf{a}_i$ . Rotational symmetry is not broken in this case. The folding of the BZ and the splitting of the bands is shown in FIG. 6c).

All angular momentum expectation values for these two states lie in the  $\text{CoO}_2$ -plane. Therefore, it is not possible to interpret these states as staggered flux states.

*spin:* The spin density order parameters  $\langle S_z^i \rangle$  for  $i = 13, 14, 15$  are invariant under time reversal symmetry. Therefore, the third order term in Eq. (38) is allowed and the transition is a first order transition.

## VII. POSSIBLE INSTABILITIES

### A. coupling constants

As can be seen from TABLE III, the coupling constants for the SDW transitions  $\Lambda^s$  are rather negative whereas the charge coupling constants  $\Lambda^c$  tend to be positive. This is not surprising as only local repulsive interaction is considered here, that tends to spread out the charge as much as possible.

The coupling constants  $\Lambda_r^{c/s}$  with  $r = 0, \dots, 3$  depend on the intra-orbital Coulomb repulsion  $U$ . As  $U$  is the largest Coulomb integral, the absolute value of these coupling constants is biggest. The remaining coupling constants  $\Lambda_r^{c/s}$  do not depend on  $U$ . For  $J' = 0$  they are also independent of  $r$ . For finite  $J'$  the degeneracy between the real (4-9) and imaginary (10-15)  $\text{SU}(4)$  generators is lifted.

In order to compare the different coupling constants better, the relations  $U = U' + 2J_H$  and  $J_H = J'$ , that hold in spherically symmetric system, can be assumed to hold approximately. The ratio  $\alpha = U'/U$  is positive and usually larger than 1/2 and smaller than 1. These assumptions allow to order the dimensionless coupling constants  $\tilde{\Lambda}^{c/s} = 9\Lambda^{c/s}/(2U)$  according to their strength. In FIG. 7 the dimensionless coupling constants  $\tilde{\Lambda}_r^{c/s}$  are shown as functions of  $\alpha$ . The most negative coupling constant is the ferromagnetic one with  $\Lambda_0^s = -6 + 3\alpha$ . For  $\alpha$  close to 1, the coupling constant for spin density order  $\tilde{\Lambda}_1^s = -(2 + \alpha)$  is comparable. Smaller but still clearly negative are also the coupling constants for the spin density angular momentum states  $\tilde{\Lambda}_{10}^s = -(1 + \alpha)$ . The coupling constants  $\tilde{\Lambda}_4^c = \tilde{\Lambda}_4^s = 1 - 3\alpha$  are also negative. Finally, the coupling constant for time reversal symmetry breaking angular momentum states  $\tilde{\Lambda}_{10}^c = 3 - 5\alpha$  and for the charge density order  $\tilde{\Lambda}_1^c = 4 - 5\alpha$  are rather positive, but can in principle also be negative if  $\alpha$  is close enough to one. In fact it is quite remarkable that for  $\alpha > 0.8$

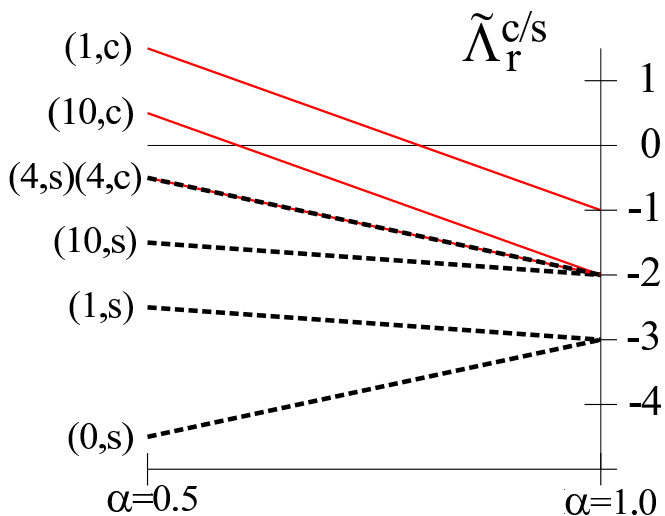


FIG. 7: The dimensionless coupling constants  $\tilde{\Lambda}_r^{c/s} = 9\Lambda^{c/s}/(2U)$  as functions of  $\alpha = U'/U$ . The relations  $U = U' + 2J_H$  and  $J' = J_H$  are assumed to hold. The solid (dashed) lines denote the charge (spin) coupling constants.

all coupling constants constants (except  $\Lambda_0^c$ ) are negative. For  $\alpha = 1$  additional degeneracies among the coupling constants appear, as can be seen in FIG. 7. This indicates the existence of a higher symmetry at this point. In fact, the local Coulomb interaction  $H_r^C$  of Eq. 15 depends only on the total charge  $n_r = \sum_{m\sigma} n_{rm\sigma}$  on the site  $\mathbf{r}$  and is given by  $Un_r(n_r - 1)/2$  for  $\alpha = 1$ .

### B. effect of the trigonal distortion

In the mean-field description, an instability occurs if the Stoner-type criterion is satisfied. At zero temperature in the system with full symmetry, this criterion reads in our notation as

$$\frac{-\Lambda_r^{c/s}}{4} D(E_F) = 1, \quad (44)$$

where  $D(E_F)$  is the density of states per spin and per hole pocket. For rather small pockets  $D(E_F)$  is given by  $\sqrt{3}/(2\pi t) \approx 0.28/t$  in our tight binding model, increases however with decreasing  $E_F$  (cf. Fig. 2). From Eq. (44) we can estimate that the critical  $U$  must be larger than  $10t$  for having a ferromagnetic instability. With the introduction of the trigonal distortion, as it was discussed in section V, the Stoner criteria of Eq. (44) are modified.

For the order parameters described by the matrices  $K^0, K^4, K^{5-6}$  and  $K^{10-12}$ , that commute with the trigonal distortion  $K^4$ , the change of the Stoner criterion is only due to the changing of the density of states at the M and the  $\Gamma$  pockets by the trigonal distortion, and the Stoner criterion is only slightly modified as long as all four pockets exist.

On the other hand, the instabilities towards states, where the order parameters with the matrices  $K^{13-15}$

are finite, would be strongly affected by the trigonal distortion, as the pocket states that hybridize in such a transition are no longer degenerate.

Finally, as mentioned above, the order parameters described by the matrices  $K^{1-3}$  and  $K^{7-9}$  transform with the same representation and are mixed by the trigonal distortion. For strong distortions the mixing tends to odd-even combinations and only the odd combinations,  $K^1 - K^7, K^2 - K^8, K^3 - K^9$  commute with the symmetry breaking field,  $K^4$ , and connects the still degenerate states of the M pockets.

If the trigonal distortion is so strong, that the pockets states at the M points lie below the FS, only a spontaneous ferromagnetic instability can still occur according to the Stoner criterion. First order transitions, however, are still possible.

The ferromagnetism is the leading instability in the symmetric model and is least affected by the trigonal distortion. Therefore, in real  $\text{Na}_x\text{CoO}_2$  systems where a rather strong trigonal distortion is unavoidably present, ferromagnetism would be most robust and is in fact the only type of all the described, exotic symmetry breaking states, that would have a chance to occur spontaneously.

However, even if the coupling constants of the more exotic states are not negative enough, to produce a spontaneous instability, their corresponding susceptibilities can be large enough to give rise to an important response of the electrons in  $\text{CoO}_2$ -plane to external perturbations. In the next section, we describe how the Na-ions can be viewed as an external field for the charge degrees of freedom.

## VIII. NA-SUPERSTRUCTURES

In  $\text{Na}_x\text{CoO}_2$  the Na-ions separate the  $\text{CoO}_2$  planes. There are two different Na-positions which are both in prismatic coordination with the nearest O-ions. The Na2 position is also in prismatic coordination with the nearest Co-ions, while the Na1 position lies along the  $c$ -axes between two Co-ions below and above. This leads to significant Na-Co repulsion, suggesting that the Na1 position is higher in energy. In fact, the Na2 position is the preferred site for  $\text{Na}_{0.75}\text{CoO}_2$ , where the ratio of occupied Na1-sites to occupied Na2-sites is about 1:2.<sup>12</sup> Deintercalation of Na does however not lead to a further depletion of the Na1-sites. On the contrary, the occupancy ratio goes to 1 for  $x$  going to 0.5. Further there is a clear experimental evidence, that at  $x = 0.5$  the Na-ions form a commensurate orthorhombic superstructure already at room temperature.<sup>8</sup> For several other values of  $x$  also superstructure formation has been reported, but  $x = 0.5$  shows the strongest signals and has the simplest superstructure.<sup>9,10</sup> In addition for  $x = 0.5$  samples a sharp increase of the resistivity at 50K respectively at 30K was reported.<sup>7,11,21</sup>

This experimental situation is rather surprising, naively one expects commensurability effects to be

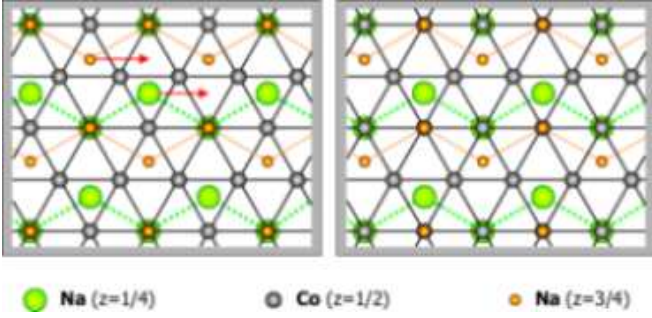


FIG. 8: Two different Na superstructures in  $\text{Na}_{1/2}\text{CoO}_2$ . The left one does not break rotational symmetry and would drive a charge ordering as shown in FIG. 5c). The right one is in fact realized in  $\text{Na}_{1/2}\text{CoO}_2$ , it is obtained from the right one by shifting the Na-chains along the arrows. This shift is due to the Coulomb repulsion of the Na-ions.

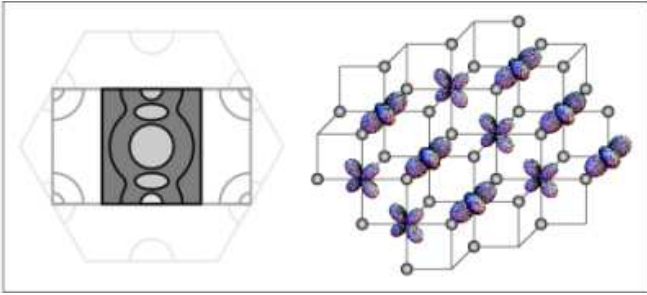


FIG. 9: The charge ordering pattern corresponding to the matrix  $K^1 - K^7$ , consists of alternating rows of  $d_x$  and  $d_y - d_z$  orbitals. On the left hand side the original BZ, the orthorhombic BZ due to the charge ordering and the experimentally observed reduced orthorhombic BZ (dark) are shown.

strongest at  $x = 1/3$  or at  $x = 2/3$  on a triangular lattice but not at  $x = 1/2$ . Therefore, it was concluded that structural and electronic degrees of freedom are coupled in a subtle manner in  $\text{Na}_x\text{CoO}_2$ .<sup>12</sup>

In this section we show how the different ordering patterns can couple to the observed Na superstructure at  $x = 1/2$ . Before going into the details, we note that due to our starting point of inter-penetrating Kagomé lattices, commensurability effects will be strongest for samples where the Na-ions can form a simple periodic superstructures that double or quadruple the area of the unitcell, since specifying a single Kagomé lattice also quadruples the unitcell. For  $x = 1/2$  such simple superstructures exist as shown in FIG. 8. A sodium superstructure couples to the charge but not to the spin degrees of freedom in the  $\text{CoO}_2$  layer. In our model, there are 15 collective charge degrees of freedom. From FIG. 7 can be seen that  $\Lambda_r^c$  is most negative for  $r = 4, \dots, 9$ . Hence, these modes are the “softest” charge modes generating the strongest response to a Na-pattern. As shown in FIG. 5, the charge order corresponding to  $r = 4, 5, 6$  does not enlarge the unitcell and does therefore not optimally couple to the Na-patterns that can be formed with

$x = 0.5$ . However the orbital pattern shown in FIG. 5c) has lobes of electron density pointing towards selected Na1 and Na2 positions. For  $x = 1/2$  it is possible to occupy all these and only these positions. This leads to the left Na-superstructure of FIG. 8. In other words, this Na-superstructure couples in a optimal way to this rotationally symmetric charge pattern. Further, the Landau expansion shows that the rotationally symmetric combination is favored by the third-order term. Therefore, it is clear that the electronic degrees of freedom would favor this Na-superstructure. This pattern however does not maximize the Na-ions distances. It is apparent that the average distances between the sodium ions can be increased, if every second of the one-dimensional sodium chains is shifted by one lattice constant as shown in FIG. 8. In this way an orthorhombic Na-superstructure is obtained, which is the one observed in experiments. This orthorhombic pattern does not drive the rotationally symmetric charge pattern shown in FIG. 5c), which is described by the matrix  $\tilde{K}^7 = K^7 + K^8 + K^9$ , it might however drive the orthorhombic charge pattern described by the matrix  $K^7$  or rather the orthorhombic charge pattern described by  $K^1 - K^7$ , as in the presence of trigonal distortion the  $K^1$  and  $K^7$  mix and the odd combination will have the most negative coupling constant. This charge pattern is shown in FIG. 9. It consists of lines of  $d_x$ -orbitals alternating with lines of the linear combination  $d_y - d_z$ -orbitals. Note, that this charge pattern corresponds to the mixed  $K^1 - K^7$ -matrix, the charge is not uniformly distributed on the Co-atoms. In this charge pattern, the Na1-sites above the  $(d_y - d_z)$  Co-sites will be lower in energy than the Na1-sites above the  $d_x$  Co-sites and similarly the Na2-positions are separated into nonequivalent rows.

In reciprocal space, such a charge ordering leads to a folding of the BZ such that the two M-pockets hybridize. The ordering of the Na-ions along the chains leads to a further folding of the BZ and to a hybridization of the bands, as it is shown in FIG. 9. The schematic FS in FIG. 9 is drawn to illustrate the hybridization occurring due to the translational symmetry breaking. Li et al. performed density-functional calculations in order to determine the band-structure of  $\text{Na}_{0.5}\text{CoO}_2$  in the presence of the orthorhombic superstructure from first-principles.<sup>49</sup> Quite generally one can assume that this superstructure, which specifies a direction on the triangular lattice, can lead to quasi-one-dimensional bands in the reduced BZ. For such one-dimensional bands, nesting features are likely to occur and would lead to a SDW-like instability, as it was observed at 53 K by Huang et al.<sup>8,33</sup> Such a transition could open a gap at least on parts of the FS and in this way lead to the drastic increase of the resistivity observed at 53 K.<sup>7</sup> At higher temperature, the resistivity is comparable in magnitude to the metallic samples and increases only slightly with lowering temperature. This weakly insulating behavior could be another effect of Na-ion ordering. Since the rotational symmetry is broken, domains can be formed. The existence of

domain walls would be an obstacle for transport where thermally activated tunneling processes play a role. It would be interesting to test this idea by removing the domains and see whether metallic temperature dependence of the resistivity would result. A bias on the domains can be given by in-plane uniaxial distortion.

To finish this section, we will discuss a further mechanism, that could lead to a non-magnetic low-temperature instability in  $\text{Na}_{0.5}\text{CoO}_2$ . In section VI we saw that the third order term in the Landau expansion, Eq. (38), favors always a rotationally symmetric charge ordering where all three order parameters  $\eta_1$ ,  $\eta_2$  and  $\eta_3$  have the same magnitude. But as argued above, the Na-ion repulsion leads nevertheless to an orthorhombic charge ordering, where only one order parameter  $\eta_1$  is finite. From Eq. (38), we obtain a Landau expansion for the remaining two order parameters  $\eta_2$  and  $\eta_3$  containing only second and fourth order terms. The second order term is given by

$$\frac{\tilde{\alpha}}{2}(\eta_2^2 + \eta_3^2) + \tilde{\beta}\eta_2\eta_3, \quad (45)$$

where

$$\tilde{\alpha} = \alpha + \left(\gamma_1 + \frac{\gamma_2}{2}\right)\eta_1^2, \quad \tilde{\beta} = \beta\eta_1. \quad (46)$$

The condition for a second order phase transition, that leads to finite values of  $\eta_2$  and  $\eta_3$  is  $\tilde{\alpha} < |\tilde{\beta}|$ . As we have  $\alpha > 0$  and linear growth of  $|\tilde{\beta}|$  and quadratic growth of  $\tilde{\alpha} - \alpha$  with  $\eta_1$ , the condition is fulfilled neither for large nor for small values of  $\eta_1$ . But for intermediate values of  $\eta_1$  it can be fulfilled. This tendency back towards the original hexagonal symmetry in this or a similar form could be responsible for the appearance of additional Bragg peaks at the intermediate temperature of 80-100K in  $\text{Na}_{0.5}\text{CoO}_2$ .<sup>8</sup> Note however, that it was speculated that these Bragg peaks only exist over a narrow range of temperature.

## IX. CONCLUSIONS

In this paper the properties of a high-symmetry multi-orbital model for the  $\text{CoO}_2$ -layer in combination with local Coulomb interaction are discussed. The tight-binding model is a zeroth order approximation to the kinetic energy, as it only includes the most relevant hopping processes using Co-O  $\pi$ -hybridization. Nevertheless it produces the hole pocket with predominantly  $a_{1g}$  character around the  $\Gamma$  point, in agreement with both LDA calculations and ARPES experiments. Furthermore, the three further pockets around the M points, although not seen in ARPES experiments, suggest that additional degrees of freedom that can not be captured in a single-band picture could be relevant. The existence of identical hole pockets in the BZ does however not produce pronounced nesting features.

The local Coulomb repulsion of the  $t_{2g}$ -orbitals can be taken into account by an effective interaction of fermions with four different flavors, associated with the four hole pockets or the four inter-penetrating Kagomé lattices. This effective interaction has a large discrete symmetry group, that allows to classify the spin- and charge-density operators, and to determine for every mode the corresponding coupling constant.

It turns out that with an effective trigonal distortion, that splits the degeneracy between the  $\Gamma$  and the M points, general corrections to the quadratic part of the Hamiltonian, such as trigonal distortion or additional hopping terms, can be taken into account, provided they are small. This effective trigonal distortion reduces the symmetry of the Hamiltonian down to the space-group symmetries of the  $\text{CoO}_2$ -plane, by breaking the gauge symmetries of the effective interaction.

Most coupling constants are negative for reasonable assumptions on the Coulomb integrals  $U$ ,  $U'$ ,  $J'$  and  $J_H$ , but the ferromagnetic coupling constant is most negative and constitutes the dominant correlation. The charge and spin density wave instabilities without trigonal distortion are easily described in a mean-field picture. In reciprocal space the degenerate bands split, and if bands belonging to different pockets hybridize, the BZ is folded. In real space different types of orderings are possible. The occupancy of the different  $t_{2g}$  orbitals on different sites can be nonuniform, resulting in a charge ordering with nonuniform charge distribution on the Co-sites. Further, certain real or complex linear combinations of  $t_{2g}$  orbitals can be preferably occupied on certain sites. In this case, the charge is uniformly distributed on the sites, but depending on the linear combinations of the orbitals, certain space group symmetries are broken. The complex linear combinations of  $t_{2g}$  orbitals have in general a non-vanishing expectation value of the orbital angular momentum.

The tendency to these rather exotic states turns out to be smaller than the ferromagnetic tendency, and this dominance of the ferromagnetic state is even more enhanced by the trigonal distortion. This is in good agreement with experiments, where ferromagnetic in-plane fluctuations have been observed by neutron scattering measurements in  $\text{Na}_{0.75}\text{CoO}_2$ .<sup>23,24</sup> There are also several reports of a phase transition in  $\text{Na}_{0.75}\text{CoO}_2$  at 22K to a static magnetic order, which is probably ferromagnetic in-plane but antiferromagnetic along the  $c$ -axis.<sup>26,28,29</sup>

In  $\text{Na}_{0.5}\text{CoO}_2$ , a periodic Na-superstructure couples directly to a charge pattern in our model and crystallizes already at room temperature, whereas simple  $\sqrt{3} \times \sqrt{3}$ -superstructures, that would correspond  $x = 1/3$  or  $x = 2/3$  do not couple.

For general values of  $x$  the disordered Na-ions provide a random potential that couples to the charge degrees of freedom. Due to the incommensurability, this does not lead to long range order, but the short range correlations will also be influenced by the charge degrees of freedom in the  $\text{CoO}_2$  layers. This interaction between the Na-

correlations and the charge degrees of freedom could be the origin of the charge ordering phenomena at room temperature and the observation of inequivalent Co-sites in NMR experiments.<sup>14,15</sup>

The overall agreement of our model with the experimental situation is good. Ferromagnetic fluctuations are dominant in our model and in experiments. Furthermore, our model is based on a metallic state and allows for charge ordering and spin density ordering transitions without changing the metallic character of the state. Finally, the clear Na superstructures, that were found at  $x = 0.5$ , can be understood quite naturally in this model.

On the other hand there are still many open questions for the cobaltates. Mainly the origin and the symmetry of the superconducting state of  $\text{Na}_x\text{CoO}_2 \cdot y\text{H}_2\text{O}$  is still under debate. Unfortunately the Na content  $x = 0.35$  is beyond the validity of the approximations made in the derivation of our model. But also the samples with  $x \geq 0.5$  have still many intriguing properties like the strongly anisotropic magnetic susceptibility, which shows the unusual Curie-Weiss temperature dependence. A possible description of the anisotropy of the magnetic susceptibility could be achieved by introducing a spin-orbit term into the kinetic energy.

We hope that our model will be useful for further understanding of the rich experimental situation of the cobaltates.

## X. ACKNOWLEDGMENTS

We thank E. Bascones, B. Batlogg, M. Brühwiler, J. Gavilano, H.R. Ott, T.M. Rice, and K. Wakabayashi for fruitful discussions. This work is financially supported by a grant of the Swiss National Fund and the NCCR program MaNEP of the Swiss National Fund.

## APPENDIX A

The equivalence of the two definitions for the "pocket operators" made in Eq. (9) and in Eq. (8) follows from

$$\begin{aligned}
b_{\mathbf{K}m}^{\dagger j} &= \frac{1}{2} \sum_l e^{i\mathbf{B}_j \cdot \mathbf{a}_l} a_{\mathbf{K}m}^{\dagger l} \\
&= \frac{1}{2} \sum_l e^{i\mathbf{B}_j \cdot \mathbf{a}_l} \frac{2}{\sqrt{N}} \sum_{\mathbf{R}} e^{i\mathbf{K} \cdot (\mathbf{R} + \mathbf{a}_l + \mathbf{a}_m)} a_{\mathbf{R}m}^{\dagger l} \\
&= e^{-i\mathbf{B}_j \cdot \mathbf{a}_m} \frac{1}{\sqrt{N}} \sum_{l\mathbf{R}} e^{i(\mathbf{K} + \mathbf{B}_j) \cdot (\mathbf{R} + \mathbf{a}_l + \mathbf{a}_m)} c_{\mathbf{R} + \mathbf{a}_l + \mathbf{a}_m m}^{\dagger} \\
&= e^{-i\mathbf{B}_j \cdot \mathbf{a}_m} c_{\mathbf{K} + \mathbf{B}_j m}^{\dagger} \tag{A1}
\end{aligned}$$

The diagonal form of the tight-binding Hamiltonian in Eq. (11) follows directly from the relation

$$c_{\mathbf{K} + \mathbf{B}_j}^{mm'} = e^{-i\mathbf{B}_j \cdot (\mathbf{a}_m - \mathbf{a}_{m'})} c_{\mathbf{K}}^{mm'}. \tag{A2}$$

## APPENDIX B

In this appendix, we provide some details concerning the derivation of the effective Hamiltonian in Eq. (19). It is convenient to treat each term in Eq. (15) separately. Let us start with the Hund's coupling.

$$\frac{J_H}{2} \sum_{\mathbf{r}} \sum_{m \neq m'} c_{\mathbf{r}m\sigma}^{\dagger} c_{\mathbf{r}m'\sigma'}^{\dagger} c_{\mathbf{r}m\sigma'} c_{\mathbf{r}m'\sigma} \tag{B1}$$

$$= \frac{J_H}{2N} \sum_{\mathbf{k}\mathbf{q}\mathbf{k}'\mathbf{q}'} \sum_{m \neq m'}^r c_{\mathbf{k}m\sigma}^{\dagger} c_{\mathbf{k}'m'\sigma'}^{\dagger} c_{\mathbf{q}m\sigma'} c_{\mathbf{q}'m'\sigma} \tag{B2}$$

$$\begin{aligned}
&= \frac{J_H}{2N} \sum_{\mathbf{K}\mathbf{K}'\mathbf{Q}} \sum_{ijkl}^r \sum_{m \neq m'} e^{i(\mathbf{B}_i - \mathbf{B}_k) \cdot \mathbf{a}_m} e^{i(\mathbf{B}_l - \mathbf{B}_j) \cdot \mathbf{a}_{m'}} \times \\
&\quad \times b_{\mathbf{K}m\sigma}^{\dagger i} b_{-\mathbf{K} + \mathbf{Q} m'\sigma'}^{\dagger l} b_{-\mathbf{K}' + \mathbf{Q} m\sigma'}^k b_{\mathbf{K}' m'\sigma}^j \tag{B3}
\end{aligned}$$

The sum over the momenta in (B2) is restricted such that  $\mathbf{k} + \mathbf{k}' - \mathbf{q} - \mathbf{q}'$  equals a reciprocal lattice vector. (B3) follows from (B2) by using the definition of the pocket operators in Eq. (8). The sum over the pocket indices is again restricted such that  $\mathbf{B}_i + \mathbf{B}_j + \mathbf{B}_k + \mathbf{B}_l$  equals a reciprocal lattice vector, whereas the sum over the momenta in the reduced BZ is simplified to an unrestricted sum over three momenta. Note that this simplification is valid for small pockets, because all the processes at the Fermi energy are kept. (Small pockets means here  $4\mathbf{K}_F < |\mathbf{B}_1|$ , this corresponds to a doping with  $x > 0.55$ ) The next step is to go from orbital operators to the band operators. Restricting ourselves to the top band and taking into account Eq. (16) we can simply substitute  $b_{\mathbf{K}m\sigma}^{\dagger j} \rightarrow \frac{1}{\sqrt{3}} b_{\mathbf{K}\sigma}^{\dagger j}$ . Now we can sum over the orbital indices in Eq. (B3) and taking into account that the sum over the pocket indices is restricted we obtain the sum

$$\sum_{m \neq m'} e^{i(\mathbf{B}_i - \mathbf{B}_k) \cdot (\mathbf{a}_m - \mathbf{a}_{m'})} = 2(4\delta_{ik} - 1) \tag{B4}$$

and for the Hund's coupling term

$$\frac{J_H}{9N} \sum_{\mathbf{K}\mathbf{K}'\mathbf{Q}} \sum_{ijkl}^r b_{\mathbf{K}\sigma}^{\dagger i} b_{-\mathbf{K} + \mathbf{Q} \sigma'}^{\dagger l} b_{-\mathbf{K}' + \mathbf{Q} \sigma}^k b_{\mathbf{K}' \sigma}^j (4\delta_{ik} - 1) \tag{B5}$$

The restriction of the sum can be dropped, if we replace  $(4\delta_{ik} - 1)$  with  $(2\delta_{ijkl} - \epsilon_{ijkl}^2 - \delta_{il}\delta_{jk} - \delta_{ij}\delta_{kl} + 3\delta_{ik}\delta_{jl})$ . The terms proportional to  $J_H$  in the interaction of Eq. (19) are now obtained by dividing Eq. (B5) into two equal parts, rewrite one directly in terms of density density operators, and rewrite the other in terms of density-density and spin-density spin-density operators using the  $SU(2)$  relation  $2\delta_{\alpha\delta}\delta_{\beta\gamma} = \delta_{\alpha\gamma}\delta_{\beta\delta} + \sigma_{\alpha\gamma} \cdot \sigma_{\beta\delta}$ . Terms which renormalize the chemical potential are dropped. All the other terms in Eq. (15) are treated in the same way.

## APPENDIX C

The symmetry group  $G$  of  $H_{\text{eff}}$  is a finite subgroup of  $U(4)$  that is generated by the permutation matrices

$\mathcal{P} \in \mathcal{S}_4$  and the diagonal orthogonal matrices  $\mathcal{D} \in (Z_2)^4$ .  $G$  is a semi-direct product of  $\mathcal{S}_4$  and the normal subgroup  $(Z_2)^4$ , this allows us to find the irreducible representations of  $G$ , cf.<sup>57</sup> The elements can be written in a unique way as  $(\mathcal{P}, \mathcal{D})$  with  $\mathcal{P} \in \mathcal{S}_4$  and  $\mathcal{D} \in (Z_2)^4$ . The product of two elements  $(\mathcal{P}, \mathcal{D}) \circ (\mathcal{P}', \mathcal{D}')$  is given by  $(\mathcal{P} \circ \mathcal{P}', \mathcal{D}'')$ . From this follows that if  $(\mathcal{P}, \mathcal{D})$  is conjugate to  $(\mathcal{P}', \mathcal{D}')$ ,  $\mathcal{P}$  is conjugate to  $\mathcal{P}'$ , and the class of  $(\mathcal{P}, \mathcal{D}) \in G$  can be labelled by the class of  $\mathcal{P} \in \mathcal{S}_4$ . The elements of  $\mathcal{S}_4$  can be classified by writing them as disjunct cyclic permutations. We label the five classes as follows:  $e=1$ ,  $f=(ab)$ ,  $g=(ab)(cd)$ ,  $h=(abc)$ ,  $i=(abcd)$ . In total there are twenty 20 classes in  $G$ . The character table is shown in TABLE V. The character corresponding to the natural representation of  $G$  by orthogonal  $4 \times 4$  matrices is  $\chi_{11}$ . The representation on the 16 dimensional space  $V$  spanned by  $Q^{0-15}$ , that was defined in section IV, acts irreducibly on the subspaces  $V^0$ ,  $V^{1-3}$ ,  $V^{4-9}$  and  $V^{10-15}$

with the characters  $\chi_0$ ,  $\chi_7$ ,  $\chi_{15}$  and  $\chi_{16}$ , respectively.

With help of Schur's Lemma, it is now easy to show that the interaction  $H_{\text{eff}}$  in the Basis  $Q^{0-15}$  is diagonal, i.e.

$$Q_{ji}^r A_{ijkl}^{c/s} Q_{kl}^{r'} = \delta_{rr'} \Lambda_r^{c/s}. \quad (\text{C1})$$

and that the coupling constant  $\Lambda_r^{c/s}$  depend only on the irreducible subspace.

As discussed in section V, the subgroup  $(Z_2)^4$  describes gauge-symmetries, that are broken in the real system whereas the subgroup  $\mathcal{S}_4$  describes the space-group symmetries. The subgroup  $\mathcal{S}_4$  consists of the classes  $e_1$ ,  $f_1$ ,  $g_1$ ,  $h_1$  and  $i_1$ . The irreducible representations of  $G$  are in general reducible for the subgroup  $\mathcal{S}_4$ . For example we have  $\chi_7 = \Gamma_5$ ,  $\chi_{15} = \Gamma_1 \oplus \Gamma_3 \oplus \Gamma_5$  and  $\chi_{16} = \Gamma_4 \oplus \Gamma_5$ .

- 
- <sup>1</sup> T. Tanaka et al., Jpn. J. Appl. Phys. **33**,L581 (1994).  
<sup>2</sup> I. Terasaki et al., Phys. Rev. B **56**, R12685 (1997).  
<sup>3</sup> T. Valla et al., Nature **417**, 627 (2002).  
<sup>4</sup> Q.H. Wang et al., Nature **423**, 425 (2003).  
<sup>5</sup> K. Takada et al., Nature **422**, 53 (2003).  
<sup>6</sup> R.E. Schaak et al., Nature **424**, 527 (2003).  
<sup>7</sup> M.L. Foo et al., Phys. Rev. Lett. **92**, 247001(2004).  
<sup>8</sup> Q. Huang et al., J. Phys.: Condens. Matter **16**, 5803 (2004).  
<sup>9</sup> H.W. Zandbergen et al., Phys. Rev. B **70**, 024101 (2004).  
<sup>10</sup> Y.G. Shi et al., cond-mat/0401052.  
<sup>11</sup> X.Z. Chen et al., cond-mat/0412299.  
<sup>12</sup> Q. Huang et al., Phys. Rev. B **70**, 184110 (2004).  
<sup>13</sup> N.L. Wang et al., Phys. Rev. Lett. **93**, 237007 (2004).  
<sup>14</sup> R. Ray et al., Phys. Rev. B **59** 9454 (1999).  
<sup>15</sup> J.L. Gavilano et al., Phys. Rev. B **69**, 100404(R) (2004).  
<sup>16</sup> P. Carretta et al., Phys. Rev. B **70**, 024409 (2004).  
<sup>17</sup> M. Brühwiler et al., cond-mat/0309311.  
<sup>18</sup> C. Bernhard et. al., Phys. Rev. Lett. **93**, 167003 (2004).  
<sup>19</sup> S. Lupi et al., Phys. Rev. B **69**, 180506R (2004).  
<sup>20</sup> L. Balicas et al., cond-mat/0410400.  
<sup>21</sup> X.H. Chen et al., cond-mat/0501181.  
<sup>22</sup> S. Lupi et al., cond-mat/0501746.  
<sup>23</sup> A.T. Boothroyd et al., Phys. Rev. Lett. **92**, 197201  
<sup>24</sup> L.M. Helme et al., cond-mat/0410457.  
<sup>25</sup> Y. Ihara et al., cond-mat/0407195.  
<sup>26</sup> T. Motohashi et al., Phys. Rev. B **67**, 064406 (2003).  
<sup>27</sup> B.C. Sales et al., Phys. Rev. B **70**, 174419 (2004).  
<sup>28</sup> J. Sugiyama et al., Phys. Rev. Lett. **92**, 017602 (2004).  
<sup>29</sup> J. Sugiyama et al., Phys. Rev. B **67**, 214420 (2003).  
<sup>30</sup> F.C. Chou et al., cond-mat/0404061.  
<sup>31</sup> G. Caimi et al., Eur. Phys. J. B **40**, 231 (2004).  
<sup>32</sup> J.L. Luo et al., Phys. Rev. Lett. **93**, 187203 (2004).  
<sup>33</sup> Y.J. Uemura et al., cond-mat/0403031 .  
<sup>34</sup> P. Mendels et al., cond-mat/0501203.  
<sup>35</sup> K. Miyoshi et al., Phys. Rev. B **69**, 132412 (2004).  
<sup>36</sup> G. Baskaran, Phys. Rev. Lett. **91**, 097003 (2003).  
<sup>37</sup> B. Kumar and B.S. Shastry, Phys. Rev. **B** 68, 104 508 (2003).  
<sup>38</sup> A. Tanaka and X. Hu, Phys. Rev. Lett. **91**, 257006 (2003).  
<sup>39</sup> M. Ogata, J. Phys. Soc. Jpn. **72**, 1839 (2003).  
<sup>40</sup> Q.H. Wang et al., Phys. Rev. B **69**, 092504 (2004).  
<sup>41</sup> C. Honerkamp , Phys. Rev. B **68**, 104510 (2003).  
<sup>42</sup> A. Ferraz et al., cond-mat/0412235.  
<sup>43</sup> W. Koshibae and S. Maekawa, Phys. Rev. Lett. **91**, 257003 (2003).  
<sup>44</sup> Y. Yanase et al., cond-mat/0407563.  
<sup>45</sup> D.J. Singh, Phys. Rev. B **61**, 13397 (2000).  
<sup>46</sup> D.J. Singh, Phys. Rev. B **68**, 020503 (2003).  
<sup>47</sup> M.D. Johannes et al., cond-mat/0403135.  
<sup>48</sup> K.-W. Lee et al., Phys. Rev. B **70**, 045104 (2004).  
<sup>49</sup> Z. Li et al., cond-mat/0403727 .  
<sup>50</sup> P. Zhang et al., Phys. Rev. B **70**,085108 (2004).  
<sup>51</sup> P. Zhang et al., cond-mat/0502072.  
<sup>52</sup> M.D. Johannes et al., cond-mat/0408696.  
<sup>53</sup> M.Z. Hasan et al., Phys. Rev. Lett. **92**, 246402 (2004).  
<sup>54</sup> H.-B. Yang et al., Phys. Rev. Lett. **92**, 246403 (2004).  
<sup>55</sup> H.-B. Yang et al.,cond-mat/0501403.  
<sup>56</sup> W.B. Wu et al., cond-mat/0408467.  
<sup>57</sup> J.P. Serre, *Linear Representations of Finite Groups*, (Springer-Verlag, New York, 1977).

#	$e_1$	$e_2$	$e_3$	$e_4$	$e_5$	$f_1$	$f_2$	$f_3$	$f_4$	$f_5$	$f_6$	$g_1$	$g_2$	$g_3$	$h_1$	$h_2$	$h_3$	$h_4$	$i_1$	$i_2$	reduction to $\mathcal{S}_4$
$\chi_1$	1	1	1	1	1	1	1	1	1	1	1	1	1	1	1	1	1	1	1	1	$\Gamma_1$
$\chi_2$	1	1	1	1	1	$\bar{1}$	$\bar{1}$	$\bar{1}$	$\bar{1}$	$\bar{1}$	$\bar{1}$	1	1	1	1	1	1	1	$\bar{1}$	$\bar{1}$	$\Gamma_2$
$\chi_3$	1	$\bar{1}$	1	$\bar{1}$	1	1	$\bar{1}$	$\bar{1}$	1	1	$\bar{1}$	1	$\bar{1}$	1	1	$\bar{1}$	$\bar{1}$	1	1	$\bar{1}$	$\Gamma_1$
$\chi_4$	1	$\bar{1}$	1	$\bar{1}$	1	$\bar{1}$	1	1	$\bar{1}$	$\bar{1}$	1	1	$\bar{1}$	1	1	$\bar{1}$	$\bar{1}$	1	$\bar{1}$	1	$\Gamma_2$
$\chi_5$	2	2	2	2	2	0	0	0	0	0	0	2	2	2	$\bar{1}$	$\bar{1}$	$\bar{1}$	$\bar{1}$	0	0	$\Gamma_3$
$\chi_6$	2	$\bar{2}$	2	$\bar{2}$	2	0	0	0	0	0	0	2	$\bar{2}$	2	$\bar{1}$	1	1	$\bar{1}$	0	0	$\Gamma_3$
$\chi_7$	3	3	3	3	3	1	1	1	1	1	1	$\bar{1}$	$\bar{1}$	$\bar{1}$	0	0	0	0	$\bar{1}$	$\bar{1}$	$\Gamma_5$
$\chi_8$	3	3	3	3	3	$\bar{1}$	0	0	0	0	1	1	$\Gamma_4$								
$\chi_9$	3	$\bar{3}$	3	$\bar{3}$	3	1	$\bar{1}$	$\bar{1}$	1	1	$\bar{1}$	$\bar{1}$	1	$\bar{1}$	0	0	0	0	$\bar{1}$	1	$\Gamma_5$
$\chi_{10}$	3	$\bar{3}$	3	$\bar{3}$	3	$\bar{1}$	1	1	$\bar{1}$	$\bar{1}$	1	$\bar{1}$	1	$\bar{1}$	0	0	0	0	1	$\bar{1}$	$\Gamma_4$
$\chi_{11}$	4	2	0	$\bar{2}$	$\bar{4}$	2	2	0	0	$\bar{2}$	$\bar{2}$	0	0	0	1	$\bar{1}$	1	$\bar{1}$	0	0	$\Gamma_1 \oplus \Gamma_5$
$\chi_{12}$	4	2	0	$\bar{2}$	$\bar{4}$	$\bar{2}$	$\bar{2}$	0	0	2	2	0	0	0	1	$\bar{1}$	1	$\bar{1}$	0	0	$\Gamma_2 \oplus \Gamma_4$
$\chi_{13}$	4	$\bar{2}$	0	2	$\bar{4}$	2	$\bar{2}$	0	0	$\bar{2}$	2	0	0	0	1	1	$\bar{1}$	$\bar{1}$	0	0	$\Gamma_1 \oplus \Gamma_5$
$\chi_{14}$	4	$\bar{2}$	0	2	$\bar{4}$	$\bar{2}$	2	0	0	2	$\bar{2}$	0	0	0	1	1	$\bar{1}$	$\bar{1}$	0	0	$\Gamma_2 \oplus \Gamma_4$
$\chi_{15}$	6	0	$\bar{2}$	0	6	2	0	0	$\bar{2}$	2	0	2	0	$\bar{2}$	0	0	0	0	0	0	$\Gamma_1 \oplus \Gamma_3 \oplus \Gamma_5$
$\chi_{16}$	6	0	$\bar{2}$	0	6	0	2	$\bar{2}$	0	0	2	$\bar{2}$	0	2	0	0	0	0	0	0	$\Gamma_4 \oplus \Gamma_5$
$\chi_{17}$	6	0	$\bar{2}$	0	6	0	$\bar{2}$	2	0	0	$\bar{2}$	$\bar{2}$	0	2	0	0	0	0	0	0	$\Gamma_4 \oplus \Gamma_5$
$\chi_{18}$	6	0	$\bar{2}$	0	6	$\bar{2}$	0	0	2	$\bar{2}$	0	2	0	$\bar{2}$	0	0	0	0	0	0	$\Gamma_1 \oplus \Gamma_3 \oplus \Gamma_5$
$\chi_{19}$	8	4	0	$\bar{4}$	$\bar{8}$	0	0	0	0	0	0	0	0	0	$\bar{1}$	1	$\bar{1}$	1	0	0	$\Gamma_3 \oplus \Gamma_4 \oplus \Gamma_5$
$\chi_{20}$	8	$\bar{4}$	0	4	$\bar{8}$	0	0	0	0	0	0	0	0	0	$\bar{1}$	$\bar{1}$	1	1	0	0	$\Gamma_3 \oplus \Gamma_4 \oplus \Gamma_5$

TABLE V: The character table for the symmetry group  $G$  of the effective Hamiltonian  $H_{\text{eff}}$ . The first line labels the classes and gives the number of elements in each class. The letters of the classes indicate classes of the subgroup  $\mathcal{S}_4$ :  $e=1$ ,  $f=(ab)$ ,  $g=(ab)(cd)$ ,  $h=(abc)$ ,  $i=(abcd)$ . The characters appearing in our effective Hamiltonian are  $\chi_1$  for  $Q^0$ ,  $\chi_7$  for  $Q^{1-3}$ ,  $\chi_{15}$  for  $Q^{4-9}$  (real matrices) and  $\chi_{16}$  for  $Q^{10-15}$  (imaginary matrices).  $\chi_{11}$  is the natural representation of  $G$  defined in section IV. The last column gives the reduction of the representations into irreducible representations of the subgroup  $\mathcal{S}_4$ , that consists of the classes  $e_1$ ,  $f_1$ ,  $g_1$ ,  $h_1$  and  $i_1$ .